TÉCNICO LISBOA

Development of a Vanadium Redox Flow Battery for Energy Storage

Gianluca Ghirlanda

Thesis to obtain the Master of Science Degree in

Energy Engineering and Management

Supervisors: Prof. Alda Maria Pereira Simões
Dr. Rui Pedro da Costa Neto

Examination Committee

Chairperson: Prof. Duarte de Mesquita e Sousa
Supervisor: Prof. Alda Maria Pereira Simões
Member of the Committee: Dr. Diogo Miguel Franco dos Santos

November 2018

Ai miei fratelli,

perchè la diversità porta sempre alla crescita personale.

Acknowledgments

I would first like to thank my supervisor prof. Alda Simões who introduced me to the Eletrochemistry subject and made me fall in love with it. I want to express my gratitude for her patience (until the very last day) and for her knowledge. My sincere thanks also go to prof. Rui Costa Neto, who provided me support everytime needed.

I thank my labmates for the stimulating discussions, for teaching me to have a good behaviour in the lab, for the late night dinners where we were working together before deadline and for the self-control everytime I spoil others' experiment. In particular Kush, Marina, Kiko, Joana, Roma, Mafalda and Mario.

Non potrei mai ringraziare abbastanza i miei genitori per il loro amore e per il loro sostegno emotivo ed economico. Grazie per aver sempre creduto nelle mie abilità. Tutto ciò non sarebbe stato possibile senza di voi. Grazie anche alla nonna e a tutto il resto della famiglia.

Special thanks to my friends that were always there to celebrate good times and to assist me in bad times and my flatmates that were always ready to cook something more for me as well. Grazie ai ragazzi di Rua Actor Vale e a Lisa, per avermi dato un tetto sopra la testa.

Ultima ma non per importanza Giulia, che è stata capace di esserci ogni volta ne avevo più bisogno.

Abstract

Vanadium Redox Flow batteries (VRFB) are electrochemical energy storage system which presents a high potential in terms of grid-scale renewable energies storage solution. A fundamental and inexpensive design for a lab-scale VRFB is presented in this work, along with the basic step for the electrolyte chemical preparation from vanadium pentoxide. The electrochemical cell has 25 cm^2 of area without any specific flow path geometry and it is assembled using raw material of easy availability and tested with different working conditions and performing acid treatment on the electrodes. It has been tested with two different concentration of active species, 0.15 M and 0.3 M of vanadium. Polarization curves, charge-discharge cycles, self-discharge curves and electrochemical impedance spectroscopy are used as tool to investigate the influence of the different working conditions and treatment on the efficiency of the electrochemical cell. The space-time test was also performed to understand the mass transport behaviour inside the cell. The outcomes from EIS exhibit an improvement with an increment of the concentration and it shows the membrane has a purely resistive behavior. Among the different conditions tested in this work, better performance were achieved using the acid treated electrode and the more concentrated electrolytes, which presented current density of 40 mA/cm^2. The cell presented an improvement with the increase of concentration in charge-discharge cycles as well as in the polarization curves and self-discharge curves.

Keywords: Vanadium Redox Flow Battery, Electrochemical Energy Storage System

Sommario

Le batterie di flusso al vanadio sono sistemi elettrochimici di accumulo di energia che presentano un alto potenziale per lo stoccaggio dalla rete elettrica di energia prodotta da fonti rinnovabili. In questo lavoro è presentata una configurazione elementare e a basso costo di una batteria di flusso al vanadio, con i fondamentali passaggi per la produzione chimica dell'elettrolita dall'anidride vanadica. La cella elettochimica non presenta nessuna specifica geometria per il passaggio del flusso dell'elettrolita e ha un'area di 25 cm^2. È costruita con materiali di facile reperibilità, è testata con differenti condizioni operative e viene inoltre effettuato un trattamento con acido solforico sugli elettrodi. La cella è stata testata con due diverse concentrazioni dell'elettrolita, 0.15 M and 0.3 M. Curve di polarizzazione, cicli di carica e scarica, curve di auto-scarica e misure di impedenza elettrochimica sono stati utilizzati come strumento investigativo per comprendere l'influenza delle differenti condizioni operative e dell'efficienza del trattamento con acido sull'efficienza della cella elettrochimica. Il test per quantificare il tempo di residenza del reagente nel reattore ha permesso di comprendere i meccanismi di trasporto di massa all'interno della cella. I risultati dello spettro di impedenza elettrochimica mostrano un miglioramento delle performance con l'aumento della concentrazione così come nelle curve di polarizzazione e mostrano che la membrana ha un comportamento puramente resistivo. Le migliori efficienze sono state raggiunte utilizzando la portata massima permessa dalla pompa, gli elettrodi trattati con acido e gli elettroliti con più concentrazione di vanadio, presentando densità di corrente pari a 24 mA/cm^2. La cella elettrochimica ha dimostrato un miglioramento utilizzando un elettrolita più concentrato nei cicli di carica e scarica così come nelle curve di polarizzazione e nella curva di auto-scarica.

Parole-chiave: Batterie di flusso al vanadio, Sistema elettrochimico per l'accumulo di energia

Resumo

As pilhas de fluxo de vanádio são sistemas de armazenamento de energia eletroquímica que têm um alto potencial para o armazenamento de energia da rede elétrica produzida a partir de fontes renováveis. Neste trabalho é apresentada uma configuração elementar e de baixo custo de uma pilha de fluxo de vanádio, com os passos fundamentais para a produção química do eletrólito a partir do pentóxido de vanádio. A célula eletroquímica não possui geometria específica para o fluxo de eletrólito e tem uma área de 25 cm^2. É construída com materiais fáceis de encontrar, testadas com diferentes condições de operação e foi testado um tratamento com ácido sulfúrico nos elétrodos. A célula eletroquímica foi testada com duas concentrações diferentes, 0.15 e 0.3 M of vanádio. Curvas de polarização, ciclos de carga e descarga, curvas de auto-descarga e medidas de impedância eletroquímica foram utilizadas como ferramenta para entender a influência das diferentes condições de operação e eficiência do tratamento com ácido na eficiência total da célula eletroquímica. O teste para quantificar o espaço-tempo foi também efetuado para entender os mecanismos de transporte de massa dentro da célula. Os resultados das medidas de impedância eletroquímica mostram uma melhoria no desempenho com o aumento da concentração e mostram que a membrana tem um comportamento puramente resistivo. A eficiência máxima foi alcançada utilizando o caudal máximo permitido pela bomba, os eletrodos tratados com ácido e o eletrólitos mais concentrados, com uma densidade de corrente de 40 mA/cm^2. A célula demonstrou uma melhoria nos ciclos de carga e descarga, bem como nas curvas de polarização e na curva de auto-descarga.

Palavras-chave: Pilhas de fluxo de vanádio, Sistema eletroquímico para armazenamento de energia

Contents

Acknowledgments V
Abstract VII
Sommario IX
Resumo XI
List of Tables XV
List of Figures XVII
Nomenclature XIX
Glossary XXIII

Introduction **1**

1 Basic concepts in electrochemical energy storage **5**
1.1 Theoretical Potential 5
1.2 Actual cell potential 7
1.2.1 Activation overpotential 8
1.2.2 Concentration overpotential 9
1.2.3 Ohmic overpotential 10
1.3 Theoretical Capacity 11
1.4 Actual capacity 11
1.5 Efficiency 12

2 Vanadium Redox Flow Batteries **13**
2.1 History of Vanadium Redox Flow Batteries 13
2.2 Working principles 14
2.2.1 Concentration and flow rate 16
2.2.2 State of charge 18
2.3 Space-time and space-time yield 19
2.4 Cost Analysis 20
2.5 State of the art and commercialization 21
2.5.1 Structure and state of the art 21
2.5.2 Commercialization, applications and field trials 27
2.6 Advantages and limitations 29

3 Implementation **31**
3.1 Equipment . . . 31
3.1.1 Electrolytes . . . 32
3.1.2 Electrochemical flow cell . . . 32
3.1.3 Peristaltic pump . . . 34
3.1.4 Piping system . . . 34
3.1.5 Potentiostat . . . 34
3.2 Testing conditions . . . 35
3.2.1 Marker experiment . . . 35
3.2.2 Polarization curves . . . 36
3.2.3 Charge and Discharge cycles . . . 37
3.2.4 Self-discharge behaviour . . . 37
3.2.5 Electrochemical Impedance Spectroscopy (EIS) . . . 37

4 Results **39**
4.1 Marker experiment . . . 39
4.2 Scan rate influence on polarization behaviour . . . 40
4.3 Polarization behaviour . . . 42
4.3.1 Flow rate influence . . . 42
4.3.2 Acid treatment influence . . . 43
4.3.3 Concentration influence . . . 45
4.4 Charge-discharge cycles . . . 46
4.4.1 Acid treatment influence . . . 47
4.4.2 Concentration influence . . . 47
4.5 Concentration influence on the self-discharge . . . 49
4.6 EIS measurements . . . 50
4.6.1 Electrochemical modelling of the cell . . . 51

5 Discussion **53**

Conclusions **57**
Perspective for future work . . . 57

References **59**

List of Tables

2.1 The vanadium ions and their correspondent salts. 17
2.2 Internal cost of a VRFB 21
2.3 Installation of VRFB for different size energy storage 29

4.1 Resistance values at different flow rate for the 0.15 M of V electrolytes with acid treated electrodes 44
4.2 Resistance values at different flow rate for 0.3 M of V solutions with acid treated electrodes 46
4.3 Average value of current, potential and energy efficiency 48
4.4 Value for the component of the EC 51

List of Figures

1.1 Example of a Tafel plot 9

2.1 Simplified scheme of VRFB 14
2.2 Example of a flow redox battery stack 16
2.3 Relation between state of charge and open circuit potential 19
2.4 VRFB cost distribution 20
2.5 Microscopic view of different carbon electrodes 22
2.6 Vanadyl sulfate ($VOSO_4$) and vanadium pentoxide (V_2O_5) 23
2.7 Effect of temperature on the solubility of V_2O_5 at different sulfuric acid concentrations . . 23
2.8 Solubility as function of temperature for different sulfuric acid concentrations from the top: V(II) and V(III) and V(IV) 24
2.9 Apparent equilibrium concentration of solutions of V(V) in 6M total sulfuric acid at different temperatures 25
2.10 Chemical structure of hydrated Nafion membrane 26
2.11 VRFB prototype installed in solar house in Thailand 27
2.12 VRFB powered electric cart 28
2.13 VRFB fuel station concept for electric buses 28

3.1 Experimental equipment 31
3.2 Different vanadium oxidation state distinguished by colors 32
3.3 Redox flow cell: front view and top view 32
3.4 Component of the electrochemical flow cell 33
3.5 SEM images of the non-treated electrode NATIONAL^{TM} Carbon Felt VGD 33
3.6 Dry NAFION®117 membrane 34
3.7 Electrochemical response of the marker experiment 35
3.8 Generic polarization curve 36

4.1 Current and charge response to the marker experiment at 150 s 40
4.2 Effect of the scan rate polarization curves 40
4.3 Example of consecutive tests at different conditions 41
4.4 Polarization curves at different flow rates with non-treated electrodes at scan rate of 10 mV/s 42

4.5 Trend of current as a function of the flow rate at 0.7 V 42
4.6 Polarization curves at different flow rates with non-treated electrodes and acid treated electrodes at scan rate of 10 mV/s 43
4.7 Trend of current as a function of the flow rate at 1 V for the non-treated and the acid treated graphite felts and the normalized plot 44
4.8 SEM image of acid treated electrodes and the non-treated at magnitude of 3000x 45
4.9 Polarization curves at different flow rates for 0.15 M and 0.3 M solutions 45
4.10 Charge-discharge cycles with non-treated electrodes 46
4.11 Charge-discharge cycles with non-treated electrodes and acid treated electrodes 47
4.12 Charge-discharge cycles with 0.15 M and 0.3 M solutions 47
4.13 Effect of consecutive tests on energy efficiency for different setups of the cell 48
4.14 Values of efficiency for different cell setups 49
4.15 Self discharge curve for 0.15 M and 0.3 M solutions and self discharge curves normalized to the time (corner) 49
4.16 Subsequent spectra of electrochemical impedance 50
4.17 Influence of active species concentration on EIS 50
4.18 Impedance of a cell mounted with a single membrane and with folded membrane 51
4.19 Equivalent circuit and fitting for 0.15 M solutions and 0.3 M solutions with flow rate of 16 mL/min 52

Nomenclature

Greek symbols

α	Symmetry coefficient
β	Tafel slope
δ	Diffusion layer thickness
ϵ	Efficiency
η	Overpotential
γ	Activity coefficient
Φ	Electric field
σ	Specific conductivity

Roman symbols

A	Cross section
a	Chemical activity
c	Concentration
D	Diffusion coefficient
E	Electromotive force, potential
e	Electron
F	Faraday constant
I	Reagent
i	Current density
J	Net flux density
j	Imaginary unit
K	Chemical equilibrium constant

L Distance between electrodes

$\dot{n}$ Molar flow rate

N General number

n Number of electron involved in the reaction

$\mathcal{P}$ Product

P Charge/discharge Power

$\dot{Q}$ Volume flowrate

Q Cell capacity

R Universal gas constant

R_{tot} Total resistance

$R_{electrolyte}$ Resistance of the electrolyte

$R_{electrode}$ Resistance of the electrodes

$R_{collectors}$ Resistance of the current collectors

$R_{membrane}$ Resistance of the membrane

T Absolute temperature

t Time

u Ionic mobility

V Volume

v Velocity of the bulk electrolyte

x Number of moles

Y_0 CPE admittance

Subscripts

$\mathcal{I}$ Electrode interface

a Activation

av Available

b Bulk

c Concentration

$cell$ Cell

ch	Charge
d	Discharge
E	Voltage
e	Electrode active area
en	Energy
i	Current
in	Inlet
j	Substance
lim	Limit
max	Maximum
min	Minimum
o	Ohmic
out	Outlet
ref	Reference condition
tan	Tank
th	Theoretical
x	Vanadium oxidation state

Superscripts

$+$	Positive charge
$-$	Negative charge
$\circ$	Standard
$start$	Initial

Glossary

BOP Balance of plant: project engineering, grid connection and system integration, installation, monitoring and controlling systems, isolation and protective devices

EC Equivalent circuit

EIS Electrochemical Impedance Spectroscopy

EPDM Ethylene-Propylene Diene Monomer

ESS Energy storage systems

LSV Linear Sweep Voltammetry

OCP Open circuit potential

OM Operation and maintenance

PCS Power conversion system: power interconnection, cabling and piping

PTFE Polytetrafluoroethylene

PV Photovoltaic systems

PVC Poly-(vinyl chloride)

SOC State of charge

STP Standard temperature and pressure. The International Union of Pure and Applied Chemistry uses 273 K and 1 bar and chemical activity equal to 1

VRFB Vanadium Redox Flow Battery

XPS X-ray photoelectron spectroscopy

Introduction

During the last years, critical problems such as air pollution and energy shortage have lead to the exploration and exploitation of renewable energies. Among those, wind and solar sources are highly promising and have reached high shares of production but they are often unpredictable and intermittent, causing the instability of the grid. In this respect, energy storage systems (ESS) are gaining increased relevance as they allow to store and provide energy as needed, playing an important role to overcome renewable energies issues.

So far, several techniques have been developed for different purposes together with their advantages and disadvantages.

Motivation and Topic Overview

The efficiency and the fast response of the ESS are important assessment parameters as well as the lifetime and the investment and operational costs. The redox flow batteries are one of the most promising technologies: they combine good efficiency, short response time, reliability and long lifetime. The energy conversion is based upon the reversible electrochemical reactions of two redox couples and they are normally dissolved in the electrolyte solutions. Unlike conventional batteries where the redox-active materials are confined inside the electrodes, the redox flow batteries sometimes referred as *reversible fuel-cells*, store energy in electrolytes that are pumped into the battery stack for energy conversion. This working mechanism avoids the electrodes from undergoing structural changes, complex redox reactions and mechanical strains, increasing their working life [1]. Several redox-active materials were utilized for redox flow batteries. The National Aeronautics and Space Administration (NASA) used Fe^{3+}/Fe^{2+} and Cr^{3+}/Cr^{2+} on the positive and negative side respectively. But the device suffered from cross contamination of active material and capacity decays [2]. In recent years the unique concept and mechanism of redox flow battery technology, namely the flowing of redox-active material and the extendable energy capacity, have attracted a great interest in developing new hybrid technologies and involving new materials. Lithium-metal based flow batteries uses lithium-metal anode which is separated from the catholyte by a membrane or when a liquid catholyte is used by a ceramic separator [3]. The concept of pump-less or membrane-less flow batteries based on different mechanism such as magnetic field-controlled transfer [4], laminar flow electrochemical cells [5] have also been reported. Metal-air batteries are considered to be promising and environmental friendly ESS that can be combined with flow systems. This can be achieved by two approaches: circulating the anode materials in the form of a slurry or a solution of the

metal and ions and supplying fresh electrolyte to increase utilization of the metal anode while eliminating by-product precipitation and preventing side reactions on the air electrode [6]. The main characteristic of these energy storage systems is the total autonomy between the installed power and the stored energy, making the technology very versatile depending on the necessities and the application field [7]. The decision is to focus the attention on the vanadium redox flow battery because this type of redox flow battery suppresses the issue of irreversible cross contamination, using only one redox-active species which is characterized by four oxidation states. One disadvantage of Vanadium redox flow batteries is the small volumetric energy storage capacity, limited by the low solubility of the active species in the electrolyte [8]. The cost of vanadium is acceptable because it is a relatively abundant material, which exists naturally in 65 different minerals and fossil fuel deposits. However, the system requires the using of expensive ion-exchange membrane, which can contribute more than 40% of the overall battery cost [9]. To overcome these limitations and promote the development of the performance, there are two main approaches: on one hand to focus the attention on the basic physical phenomena behind its operation, on the other hand develop specific components designed to satisfy the precise needs of redox flow batteries. Since it is a novel technology, the actual knowledge for both approaches has not reached a total comprehension of the phenomena in order to follow a conscious optimization of the battery parameters. The room for improvement is still wide.

Objectives

The objective of the present work aims to acquire knowledge and experience on the assembly of redox flow batteries and observe the operating conditions on laboratory scale in order to understand the steps behind the design of redox flow batteries on larger scale, from safety issues to its configuration. The idea is developed from the choice of the components of the electrochemical reactor to the electrolyte production method, in order to maintain the costs as low as possible. Thereafter the cell is tested in order to assess its performance and efficiency.

Thesis Outline

The present work is organized as following:

- Chapter 1: The basics of Electrochemistry behind the energy storage systems are explained in order to give the reader a fundamental knowledge behind the device working principles.
- Chapter 2: A general overview regarding the actual state of vanadium redox flow cell and the material of which those are made is presented, explaining the working principles, advantages and disadvantages and some of their applications.
- Chapter 3: The system used is described and the conditions how the experiments were performed are explained.

- Chapter 4: The outcomes of the tests are presented, with a particular attention on the behaviour of the system at different working conditions, giving a explanation of the phenomena behind the results.
- Chapter 5: A general discussion and a comparison among the results and the outcomes reported in the literature.

Chapter 1

Basic concepts in electrochemical energy storage

An electrochemical energy storage is a technology which allows to convert chemical energy into electrical energy. It happens through an electrochemical oxidation-reduction reaction. These devices are commonly named batteries. *They can be classified in two main categories: primary and secondary. The difference consists whether the battery can be recharged or not. The energy conversion in a primary battery is irreversible and it is discarded after its energy has been utilized. On the other hand, a secondary battery can be recharged supplying electric current, restoring the battery to its original status* [10]. In the modern time, batteries are developed in different shapes, configuration and sizes. Regardless of the size and shape, the unit is called electrochemical cell or battery. During the discharging process, oxidation reaction occurs at the negative electrode, releasing electrons to power an external load and recombine in the positive electrode through a reduction reaction, where the charge carriers are released to pass through the electrolyte and the separator to the negative. The driving force is the chemical potential difference between the positive and the negative and electrons flow to generate a current opposite to the ionic current into the cell [11]. During the cell charge, external potential is applied in order to make the electrons moving in the opposite direction, converting electric energy into chemical energy [10].

1.1 Theoretical Potential

In an electrochemical cell, the total cell reaction is composed of two half reaction independent to each other that describe the chemical change in both electrodes. Contrary to usual chemical reaction that consist only transformation of chemical substances, electrochemical reactions involve transfer or charged species, such as ions and electrons, between the electrode and the electrolyte. Electrode reactions are heterogeneous and take place at the electrode-electrolyte interface. The interfacial potential is the driving force for charge transfer and it affects the process of the electrode reaction. The cell potential will result in the sum of the interfacial potentials of the cathode and the anode and it is a fundamental parameter in electrochemistry [11]. The cell potential is associated to the Gibbs free energy change in the cell and

its theoretical value can be determined through electrochemical thermodynamics. The decrease in Gibbs free energy of the electrochemical cell equals the maximum electrical energy supplied by the cell, as shown in Equation 1.1 [10]

$$\Delta G = -nFE \tag{1.1}$$

where n is the number of electrons involved in the cell reaction; F is Faraday's constant 96 485 C/mol; E is the electromotive force. Each half reaction has the same relationship between the Gibbs free energy and its electrode potential. When all the reagents and the products in the reaction are in standard condition STP:

$$\Delta G^{\circ} = -nFE^{\circ} \tag{1.2}$$

where E° is the standard potential of the cell and is related to the standard Gibbs free energy change ΔG° according to Equation 1.1.

Considering the following half reaction:

$$\sum \mathrm{x}_j \mathrm{I}_j + \mathrm{ne}^- \longleftrightarrow \sum \mathrm{x}_j \mathrm{P}_j$$

where x_j is the stoichiometric coefficient for each substance, I are the reagents and P are the products. According to the thermodynamics the change in Gibbs free energy in the electrode reaction is given by Equation 1.3 [12]

$$\Delta G_{\text{electrode}} = \Delta G^{\circ}_{\text{electrode}} + RT\ \ln(K_{\text{electrode}}) = \Delta G^{\circ}_{\text{electrode}} + RT\ \ln\left(\frac{a_{P_i}^{v_i}}{a_{I_i}^{v_i}}\right) \tag{1.3}$$

where $\mathrm{K}_{electrode}$ is the chemical equilibrium constant of the electrode reaction; a is the activity and v is the number of mole of each reactant; T is the absolute temperature; R is the universal gas constant 8.314 J/K mol. Combining Equation 1.1 and Equation 1.3:

$$E_{\text{electrode}} = E^{\circ}_{\text{electrode}} - \frac{RT}{nF} \ln \frac{a_{P_i}^{v_i}}{a_{I_i}^{v_i}} \tag{1.4}$$

This is the Nernst equation, as one of the most important equation of electrochemistry, the Equation 1.4 gives a relationship between the equilibrium potential of the electrode and the activity of the substances involved [11]. The Nernst equation is referred to with respect to a reference electrode, the SHE (standard hydrogen electrode) of which its potential has been declared zero volts [12]. There are other reference electrodes, such as SCE (saturated calomel electrode), silver-silver chloride electrode (Ag/AgCl), but when they are used the electrode potential is shifted to a different value even though the effect of the activities of the active species is the same. At 25° C the term $\frac{RT}{F}$ can be considered constant and using a base 10 logarithm the Nernst equation can be written as [13]:

$$E_{\text{electrode}} = E^{\circ}_{\text{electrode}} - \frac{0.059}{n} \log \frac{a_{P_i}^{v_i}}{a_{I_i}^{v_i}} \tag{1.5}$$

The electromotive force of the cell is the difference between the electrode potential of the cathode and the anode reaction, both obtained from the corresponding Nernst equation [11]:

$$E_{\text{cell}} = E_{\text{cathode}} - E_{\text{anode}} \tag{1.6}$$

The activity and the concentration are different and their relation is defined as [12]:

$$a = \gamma c \tag{1.7}$$

where γ is the activity coefficient that is function of the concentration of the solution. In very diluted solution, $\gamma \approx 1$. Since the activity coefficient is almost always indeterminable, the concentration is used instead and the Nernst equation then becomes [10]:

$$E_{\text{electrode}} = E^{\circ}_{\text{electrode}} - \frac{RT}{nF} \ln \frac{c_{P_i}^{v_i}}{c_{I_i}^{v_i}} \tag{1.8}$$

1.2 Actual cell potential

The theoretical potential is based on electrochemical cells in equilibrium. In reality, electrochemical cells working conditions are deviated from the equilibrium and this leads the actual cell potential E to change from the value E° in STP. This phenomenon is called polarization and the generated overpotential η is expressed as [13]:

$$\eta = E - E^{\circ} \tag{1.9}$$

The magnitude of the overpotential is related to several factors: electrode shape and size, electrolyte composition and concentration, cell architecture, temperature, etc.
The electrode reaction takes place at the interface between the electrolyte and the electrode and it can include part of all of the following electrochemical steps:

- Mass transport of reactant from the bulk electrolyte to the interface;
- Surface conversion before the electron transfer, such as chemical reactions, adsorption to the electrode surface;
- Electron transfer at the electrode surface;
- Surface conversion after the electron transfer, such as chemical reactions, desorption from the electrode surface;
- Mass transport of the products from the electrode surface to the bulk electrolyte;

The slowest process among them, namely rate-determining process, dominates the kinetic of the electrode reaction [13]. The overpotential can be divided into three types and the total overpotential of the cell is expressed as:

$$\eta = \eta_a + \eta_c + \eta_o \tag{1.10}$$

Where η_a is the activation overpotential, η_c is the concentration overpotential and η_o is the ohmic overpotential [14].

1.2.1 Activation overpotential

Activation overpotential is the potential difference required to overcome the activation energy of the cell reaction to produce current. It can be due to the electrons accumulation at the electrode surface that causes a barrier for the incoming electrons [13]. Assuming the generic reaction:

$$\mathrm{xI} + \mathrm{ne}^- \longleftrightarrow \mathrm{xP}$$

The relationship between the activation overpotential η_a and the current i is given by the Butler-Volmer equation [11]:

$$i = i_o \left[\mathrm{e}^{-\frac{\alpha n F \eta_a}{RT}} - \mathrm{e}^{-\frac{(1-\alpha)\mathrm{nF}\eta_a}{\mathrm{RT}}}\right] \tag{1.11}$$

where i_o is the equilibrium exchange current, α is the transfer coefficient. The first term in Equation 1.11 is the rate of the anodic reaction and the second term is the rate of the cathodic reaction. The equilibrium current affects the intrinsic rate of the electron transfer of the reaction. According to Faraday's law that states *the amount of substance produced at each electrode is directly proportional to the quantity of charge flowing through the cell*, the lower the exchange current the slower the electrode reaction. The transfer coefficient indicates when the electrode reaction favors the anodic or cathodic direction at a given applied potential [10]. If the overpotential is small, according to Taylor series of the exponential function, the Equation 1.11 can be approximated as:

$$i = \frac{i_o n F}{RT}\,\eta_a \tag{1.12}$$

which denotes a linear dependence between the current and the activation overpotential in the equilibrium potential range. At high activation overpotential typically above 100 mV, both positive or negative, one of the two terms in the Equation 1.11 is negligible and the equation becomes:

$$i = i_o\,\mathrm{e}^{-\frac{\alpha n F \eta_a}{RT}} \tag{1.13}$$

Rearranging the Equation 1.13 in another form:

$$\eta_a = \frac{RT}{\alpha n F}\ln i_o - \frac{RT}{\alpha n F}\ln i = 2.303\left(\frac{RT}{\alpha n F}\log i_o - \frac{RT}{\alpha n F}\log i\right) = \beta \log\left(\frac{i}{i_0}\right) \tag{1.14}$$

The exponential relation between current and activation overpotential is called Tafel equation [11]. The term β is the Tafel slope, which shows how the overpotential changes in function of the logarithm of the current density expressed in V.

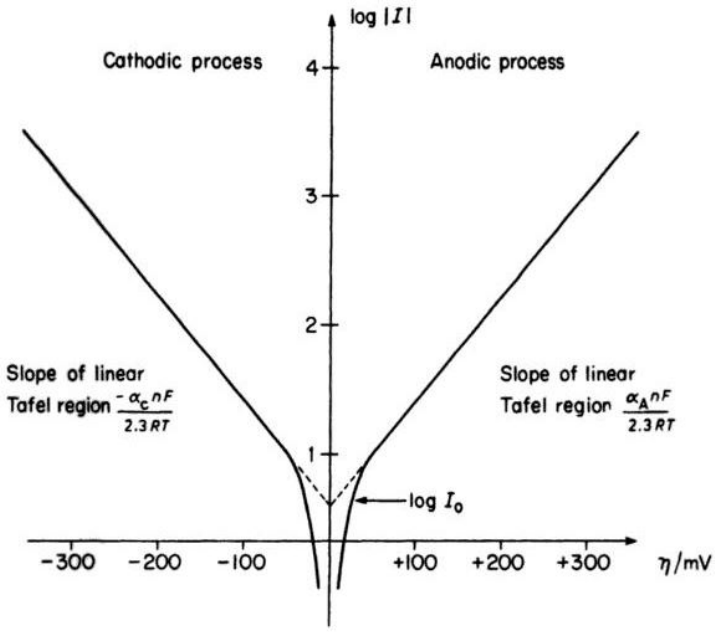

Figure 1.1: Example of a Tafel plot [11]

1.2.2 Concentration overpotential

Concentration overpotential is caused by the gradient of concentration of the reacting substances on the electrode surface and in the bulk electrolyte. It occurs when the rate of reaction is fast and the mass transport is relatively slow [11]. For this reason, the reacting molecules cannot reach the reaction site and it results in depletion of reactant. The same concept is valid for the product molecules, resulting in accumulation of the product on the electrode surface [13]. The mass transport is usually carried out through:

- Migration of charged species due to the presence of an electric field;
- Diffusion, from high to low concentration areas;
- Convection imposed by the unbalance of forces on the electrolyte, such as density gradient or stirring;

Applying an external forced convection can facilitate mass transport of the electroactive material in the cell [11]. The mass transport from the bulk electrolyte to the electrode surface is regulated by Nernst-Planck equation [13]:

$$J_j = -D_j \nabla c_j - u_j c_j \nabla \Phi + v c_j \tag{1.15}$$

The first term of the equation is related to the contribution of diffusion, the second term represent the migration and the last one is the convection term. In particular, J_i is the net flux density of the species j, D_i is the diffusion coefficient [$cm^2\ s^{-1}$], ∇c_j is the concentration gradient; u_j is the ionic mobility that describes how fast the ions react to the electric field, $\nabla\Phi$ is the gradient of the electric field; v is the velocity of the bulk electrolyte.

When the reaction is controlled by diffusion and the electron transfer kinetics are rapid, the concentration of the reagents close to the electrode/solution interface decreases as the current increases with this relation [10]:

$$i = \frac{nFD}{\delta}\left(c_b - c_i\right) \tag{1.16}$$

At specific value of current, the reagents are converted once they are close to the electrode surface, therefore its concentration tends to zero. This is the limiting current, at which the maximum rate of the reaction is reached [10]. The limiting current density is [11]:

$$i_{lim} = \frac{nFD}{\delta}\, c_b \tag{1.17}$$

D is the diffusion coefficient of the reagents, c_b is the concentration of the reagents in the bulk and δ is the diffusion layer thickness, a region where the concentration of reagents is different from the bulk electrolyte. Combining Equation 1.17 and Equation 1.16 at specific current density i the concentration of reagents c can be expressed as:

$$c = \frac{i_{\text{lim}} - i}{i_{\text{lim}}}\, c_b \tag{1.18}$$

If the transfer by migration is negligible and the ratio between the ionic activity coefficient is assumed to be unity, then the resulting concentration overpotential for a generic electrode reaction will be [13]:

$$\eta_c = E - E^\circ = \frac{RT}{nF} \ln\left(\frac{c_i}{c_b}\right) \tag{1.19}$$

Combining Equation 1.18 and Equation 1.19 the concentration overpotential can be obtained in dependence of current density [10]:

$$\eta_c = \frac{RT}{nF} \ln\left(1 - \frac{i}{i_{\text{lim}}}\right) \tag{1.20}$$

During operation of the cell, the concentration in the bulk can be assumed as homogeneous. A stagnant layer of electrolyte of thickness δ is supposed to exist between the electrode surface and the bulk electrolyte, where the mass transfer is achievable only by migration and diffusion. The thickness of the diffusion layer δ depends only on the hydrodynamic conditions and the viscosity of the solution [15].

1.2.3 Ohmic overpotential

The ohmic overpotential is related to the movement of electrical charges and its concept is similar to the mechanical notion of friction. It is due to electric resistance, the ability of a media to impede the flow of charges, both electrons and ions. This overpotential is described through Ohm's Law:

$$\eta_o = iR_{\text{tot}} \tag{1.21}$$

Therefore, the ohmic overpotential is linearly dependent onf the applied current. In particular the

ohmic resistance Ω is the sum of the electric resistance of the electrodes and the current collector plates. The membrane that separates the anolyte and the catholyte has also a resistance opposing the flow of charges, namely protons. The electrolyte is also characterized by a resistance that varies with the salt composition and its concentration. In particular it is defined as [10]:

$$R_{\text{electrolyte}} = \frac{L}{\sigma\, A_{\text{electrode}}} \tag{1.22}$$

where L is the length between the two electrodes, A is the cross-section of the electrodes and σ is the specific conductivity. It has direct relationship with number, charge and mobility of the ions inside the electrolyte. Then the Equation 1.21 can be written as:

$$\eta_o = (R_{\text{electrodes}} + R_{\text{collectors}} + R_{\text{electrolyte}} + R_{\text{membrane}})\, i \tag{1.23}$$

1.3 Theoretical Capacity

The theoretical capacity of a electrochemical cell is defined as the number of the electric charge present in the cell, expressed in Coulomb (C) or Ampere-hours (Ah) and it corresponds to the maximum amount of energy that can be stored in the cell. It is determined from Faraday's law:

$$Q_{\text{th}} = xnF \tag{1.24}$$

where n is the number of transferred electrons, F is the Faraday's constant and x is the number of moles of a specific electroactive material involved in the cell reaction [10]. In redox flow batteries, the capacity is usually expressed as volumetric specific capacity, since the electroactive material is contained in the electrolytes and stored in tanks. In reality, the full theoretical capacity can never be achieved, because a 100% utilization of the electroactive material in a cell is impossible [16].

1.4 Actual capacity

The actual charge capacity is lower than the theoretical capacity for several factors. The cell capacity is very dependent on charge/discharge rate. The cell capacity decreases when high currents are involved due to the increase in overpotential. Furthermore, side reaction occurs on the electroactive material reducing the cell capacity, for example hydrogen evolution at negative electrode of VRFB. The actual cell capacity depends on the cell charge/discharge mode. With constant current applied [10]:

$$Q = i \cdot t \tag{1.25}$$

where i is the current and t is the time. With a constant applied potential the capacity is expressed as:

$$Q = \int_0^t i\, dt \tag{1.26}$$

If the power is constant then Equation 1.26 becomes:

$$Q = \int_0^t i\,dt = P \int_0^t \frac{1}{E_{\text{cell}}}\,dt \tag{1.27}$$

Where E_{cell} is the cell potential and P is the charge/discharge power .

1.5 Efficiency

The performance of a battery is evaluated through its efficiency. The current efficiency is the ratio between the discharge capacity and the charge capacity [10]:

$$\eta_{\text{i}} = \frac{Q_{\text{d}}}{Q_{\text{ch}}} = \frac{\int_{t_{\text{d}}}^{t_{\text{ch}}} i_{\text{d}}\,dt}{\int_0^{t_{\text{ch}}} i_{\text{ch}}\,dt} \tag{1.28}$$

It describes the electron transfer performance and it takes into account the side reactions and the crossover, that is the reduction of the battery's capacity and the imbalance of the solution due to the active species crossing through the membrane. For this reason the current efficiency results higher when high current densities are involved, because the ions have less available time to cross the membrane.
The potential efficiency is defined the ratio between the average potential during the discharge and during the charge of the battery [17]:

$$\eta_{\text{E}} = \frac{\overline{E}_{\text{d}}}{\overline{E}_{\text{ch}}} = \frac{\int_{t_{\text{d}}}^{t_{\text{ch}}} E_{\text{d}}\,dt}{\int_0^{t_{\text{ch}}} E_{\text{ch}}\,dt} \tag{1.29}$$

This parameter takes into account the losses due to the overpotentials. The current efficiency decreases when the current density increases because it intensifies the ohmic losses.
The energy efficiency is the product between the two precedent parameters and it describes the overall performance of the battery [10]:

$$\eta_{\text{en}} = \eta_{\text{i}}\,\eta_{\text{E}} = \frac{\int_{t_{\text{d}}}^{t_{\text{ch}}} P_{\text{d}}\,dt}{\int_0^{t_{\text{ch}}} P_{\text{ch}}\,dt} = \frac{\int_{t_{\text{d}}}^{t_{\text{ch}}} E_{\text{d}}\,i_{\text{d}}\,dt}{\int_0^{t_{\text{ch}}} E_{\text{ch}}\,i_{\text{ch}}\,dt} \tag{1.30}$$

To optimize the performance of the battery is necessary to consider the effect of each intervention in both efficiency parameters and to not neglect any undesired phenomena during the operation of the battery.

Chapter 2

Vanadium Redox Flow Batteries

In this chapter the history of the battery is presented and then the basic principles of the vanadium redox flow battery together with its structure and basic components are described. The next sections will also show the cost analysis, the main applications and the marketability and the state of the art of the technology. The chapter ends giving a general overview between its advantages and disadvantages.

2.1 History of Vanadium Redox Flow Batteries

The flow batteries are modern devices, but nowadays they gain a significant interest because of the introduction of the renewable energies in the world's energy scenario. Due to the growing production of energy from renewable sources the need of efficient and long-lasting energy storage systems, which guarantee a sure and stable electric grid management and this type of batteries are well suited for those purposes. The first flow battery was developed by Charles Renard in 1884 and placed on an airship and the reagent involved were chlorine and zinc. The use of vanadium as reagent was proposed for the first time in 1933 by Pissoort [18] and after by Pelligri e Spaziante in 1978 [19]. Meanwhile, researchers from NASA were interested on the aerospace application of redox flow batteries from the beginning of the 1970's. The first prototype of vanadium redox flow battery with acid solution was realized by M. Skyllas-Kazacos and her colleagues in 1980s at the University of New South Wales [20] and patented in 1986 [21]. The interest on the new technology was lost afterwards due to its poor ability to compete on the market compared to other batteries, in particular for mobile application. Only lately, because of the electric grid stability problem due to renewable energies introduction, the vanadium redox flow batteries have been reconsidered because they might offer interesting performance. An example of recent improvement is the mixed acid solution electrolyte developed by the Pacific Northwest National Laboratory in 2015 which allows the battery to operate on a wider range of temperature and permits to double the energy density of the system [22]. At the same time, different redox couple were investigated, in order to optimize the performance and avoid weaknesses, such as Zinc-Bromine, Iron-Chromium, vanadium-Bromine and vanadium-Oxygen [23].

2.2 Working principles

The redox flow batteries are electrochemical devices able to convert chemical energy from electrolytes into electrical energy and vice versa, through a redox reaction. For this reason the electrolytes are essential components of the battery. They are stored inside tanks and they flow into the cell through the porous electrodes, where the reactions take place and the charge is transferred. The released electrons flow into an external electric circuit and they determine the continuous current supplied or absorbed from the battery. The two electrolyte are always separated from each other, due to the presence of the proton exchange membrane. It allows the proton transfer from one half-cell to the other. This work focuses the attention on the all vanadium redox flow batteries (VRFB), even though the principles are in compliance with other typologies. The basic working scheme during carge and discharge is shown in Figure 2.1.

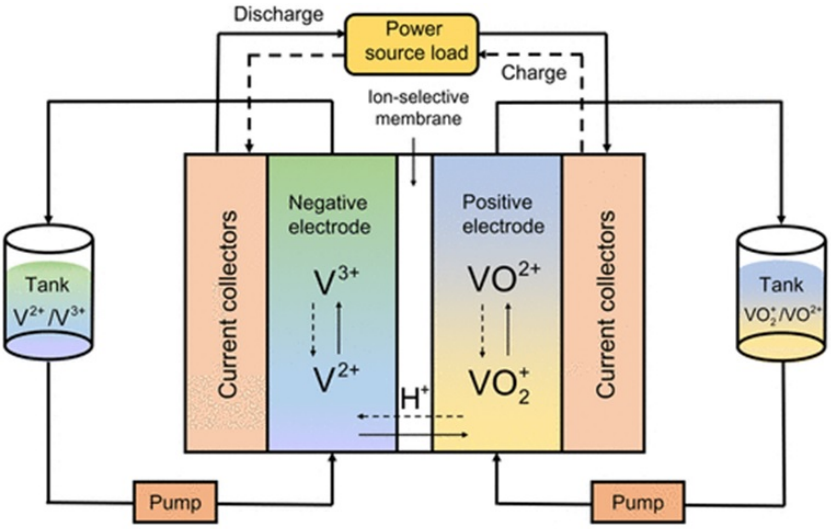

Figure 2.1: Simplified scheme of VRFB [24]

The electrolytes are composed of vanadium ions dissolved in sulfuric acid and water. They are pumped from the storage tanks into the respective half cell and in discharge mode, the oxidation reaction takes place at the anode with the release of one electron while the reduction takes place at the cathode where the electron is absorbed. The electrons are transferred from the porous carbon electrode toward the current collector through the graphite plates, on which the flow field distribution is engraved. Proton exchange membranes are used to separate the two electrolytes, usually Nafion. The redox reactions involve the four different vanadium oxidation states, at which correspond different colors. At anode the couple V^{2+}/V^{3+} and at the cathode the couple VO_2^+/VO^{2+}, namely V^{5+}/V^{4+}.

The reactions are listed below, the anode and the cathode respectively.

Negative half-cell reactions:

$$V_{aq}^{3+} + e^- \longrightarrow V_{aq}^{2+} \text{ (charge)}$$

$$V_{aq}^{2+} \longrightarrow V_{aq}^{3+} + e^- \text{ (discharge)}$$

Positive half-cell reactions:

$$VO^{2+}_{aq} + H_2O \longrightarrow VO^{+}_{2\,aq} + 2H^+ + e^- \text{ (charge)}$$

$$VO^{+}_{2\,aq} + 2H^+ + e^- \longrightarrow VO^{2+}_{aq} + H_2O \text{ (discharge)}$$

The overall reaction is:

$$V^{2+}_{aq} + VO^{+}_{2\,aq} + 2H^+ \longleftrightarrow V^{3+}_{aq} + VO^{2+}_{aq} + H_2O \tag{2.1}$$

From left to right in discharge mode while in the opposite sense is charging mode. The two moles of protons are transferred from one half-cell to the other inside the cell and so the use of a membrane is needed. From the reactions can be noticed not only the vanadium oxidation state changes during the charge or discharge process, but also the pH of the electrolyte solutions.
But the reactions above are not the only reactions during the operation of the cell. There are several side reactions taking place in the cell, decreasing the efficiency of the system [25] The main side reactions are hydrogen and oxygen evolution respectively:

$$2H^+ + 2\,e^- \longrightarrow H_{2(g)} \qquad (0\,V)$$

$$2\,H_2O \longrightarrow O_{2(g)} + 4\,e^- + 4H^+ \qquad (-0.827\,V)$$

Fortunately the kinetics of the side reactions become relevant only under high current densities and therefore in this work they will be neglected.
The standard potential of the cell in standard conditions is given by Equation 1.6, respectively:

$$E^{\circ}_{\text{cathode}} = 1.004\,V$$

$$E^{\circ}_{\text{anode}} = -0.255\,V$$

$$E^{\circ}_{\text{cell}} = E^{\circ}_{\text{cathode}} - E^{\circ}_{\text{anode}} = 1.259\,V$$

The applications require the cells to be assembled in series to provide higher potential in order to meet the load demand. To do so bipolar plates are collocated between the single cells, in order to separate one from the other. The bipolar plate acts as the current collector between the positive electrode for one cell and the negative electrode for the other. The cells of a stack are electrically connected in series, while the electrolytes flow in parallel. The anolyte and the catholyte inside a cell are separated by the membrane. An example of a redox flow battery stack is presented in Figure 2.2.

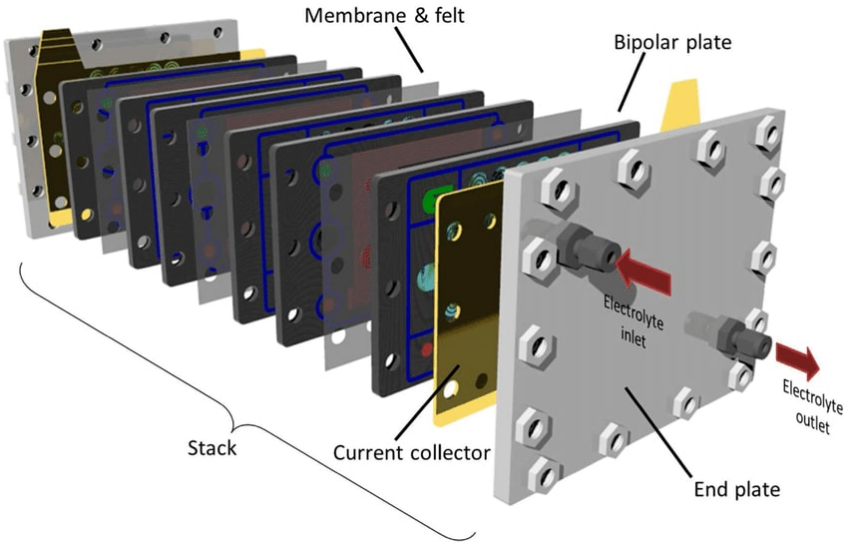

Figure 2.2: Example of a flow redox battery stack [26]

2.2.1 Concentration and flow rate

An important parameter for the VRFB is the concentrations of vanadium ions. They are not uniformly distributed along the electrolyte circuit and according to [17] four concentrations can be identified: the tank concentration, the concentration at the cell input, the concentration inside the cell and the concentration at the cell output. The same concentration is assumed between the tank and the input of the cell. The tank concentration accounts of the output of the battery and the output concentration is proportional the current. For the x species of vanadium the cell inlet concentration is expressed as:

$$c_{\mathrm{in_x}} = c_{\mathrm{tan_x}} = c_{\mathrm{tan_x}}^{\mathrm{start}} + \frac{1}{V_{\mathrm{tan}}} \int \frac{b}{F} \cdot A_e \, i(t) \, dt \tag{2.2}$$

Where c_{in_x} and c_{tan_x} are the input concentration and the tank concentration, $c_{tan_x}^{start}$ is the initial concentration of the tank, V_{tank} is the volume of the electrolyte solutions in the tank and A_e is the active area of the cell. Since the output concentration depends on several factors such as the current, the electrolytes flow rate and the length of the electrolyte circuit, it is very difficult to evaluate. In almost steady state, where current and flow rate are constant, in a single cell system and assuming the cell has no memory and reacts instantaneously to the change in operation conditions the output concentration for the x species of vanadium is [17]:

$$c_{\mathrm{out_x}} = c_{\mathrm{in_x}} + \frac{b \cdot N_{\mathrm{cells}}}{F \, \dot{Q}} \cdot i \, A_e \tag{2.3}$$

Where b is a sign factor which takes into account the reactants or products:

$$\left\{ \begin{array}{ll} 1 & \text{for } V^{2+} \text{ and } V^{5+} \text{ ions} \\ -1 & \text{for } V^{3+} \text{ and } V^{4+} \text{ ions} \end{array} \right\}$$

The concentration that will affect the OCP and consequently the one used in Equation 1.8 corresponds to the cell concentration, which cannot be evaluated because it is not uniformly distributed. In this case as there are no flow path geometry the concentration will not vary much.

Concentration of protons

The Reaction 2.1 is not exactly the reaction occurring in the cell. The electrolytes are not only composed of vanadium ions, but also sulphate ions SO_4^{2-} that are not shown in the overall chemical reaction (2.1). These ions are called supporting ions and they do not take part in the reaction but they are important to respect the law of conservation of mass and the charge balance in both electrolytes [16]. This is important to understand why the protons must cross the membrane in order to balance the charges. In Table 2.1 the vanadium ions and their salts are presented.

Table 2.1: The vanadium ions and their correspondent salts [17].

Species	**Salt**	**Electrolyte**	**State**
V^{2+}	VSO_4	Anolyte	Charged
V^{3+}	$0.5V_2(SO_4)_3$	Anolyte	Discharged
V^{4+} or VO^{2+}	$VOSO_4$	Catholyte	Discharged
V^{5+} or VO_2^+	$0.5\ (VO_2)_2SO_4$	Catholyte	Charged

In charge mode the full ionic equations for the anode and the cathode respectively:

$$V_2(SO_4)_3 + H_2SO_4 + 2H^+ + 2\,e^- \longrightarrow 2\,VSO_4 + 2\,H_2SO_4 \tag{2.4}$$

$$2\,VOSO_4 + H_2SO_4 + 2\,H_2O \longrightarrow (VO_2)_2SO_4 + 2\,H_2SO_4 + 2H^+ + 2\,e^- \tag{2.5}$$

It is evident that the half-cell Reaction 2.4 needs 2 moles of protons and they come across the membrane from half-cell Reaction 2.5.

Flow rate

The flow rate of the vanadium electrolyte is very important because it affects the rate of electrons to be released, and consequently the potential of the battery and the SOC and it is related to the concentrations as shown in Equation 2.3. For a single cell system, the flow rate can be expressed as [16]:

$$\dot{Q} = \frac{i \cdot A_e}{F} \tag{2.6}$$

In order to avoid stagnation and the lack of electroactive vanadium ions, the minimum flow rate must be known. It depends on the required amount of electroactive species and on the input concentrations which either can be produced or consumed. The minimum flow rate can be derived from Equation 2.3:

$$Q_{\min}^{\text{produced}} = \frac{b \cdot i\, A_e}{F(c_{\text{out}_{\max}} - c_{\text{in}}^{\text{produced}})} \tag{2.7}$$

$$Q_{\text{min}}^{\text{consumed}} = \frac{b \cdot i\, A_e}{F(c_{\text{out}_{\text{min}}} - c_{\text{in}}^{\text{consumed}})} \tag{2.8}$$

The limiting species depends on the working mode either charge or discharge, so the minimum flow rate will be the maximum between the Equation 2.7 and Equation 2.8.

2.2.2 State of charge

The state of charge is the equivalent of a fuel gauge in a car: it indicates how much energy is stored in the battery. It varies from 0 to 1, totally discharged and totally charged respectively. When the total vanadium ions concentrations are the same for both electrolytes, the the state-of-charge (SOC) in relation with the vanadium ion concentrations is given by [27]:

$$SOC = \left(\frac{c_{\text{V}^{2+}}}{c_{\text{V}^{2+}} + c_{\text{V}^{3+}}}\right) = \left(\frac{c_{\text{V}^{5+}}}{c_{\text{V}^{5+}} + c_{\text{V}^{4+}}}\right) \tag{2.9}$$

The relations between the concentrations of each species can be written as:

$$c_{\text{V}^{5+}} = c_{\text{V}_{\text{tot}_\text{c}}} - c_{\text{V}^{4+}} \tag{2.10}$$

$$c_{\text{V}^{2+}} = c_{\text{V}_{\text{tot}_\text{a}}} - c_{\text{V}^{3+}} \tag{2.11}$$

When Equation 2.10 and Equation 2.11 are combined with Equation 2.9 the state of charge becomes:

$$SOC = \left(\frac{c_{\text{V}^{2+}}}{c_{\text{V}_{\text{tot}_\text{a}}}}\right) = \left(\frac{c_{\text{V}^{5+}}}{c_{\text{V}_{\text{tot}_\text{c}}}}\right) \tag{2.12}$$

However this formulation is not valid if the concentration of vanadium ions varies in each electrolyte. A generic formulation of SOC can be expressed as [27]:

$$SOC = \left(\frac{c_{\text{V}^{2+}} + c_{\text{V}^{5+}}}{c_{\text{V}^{2+}} + c_{\text{V}^{3+}} + c_{\text{V}^{4+}} + c_{\text{V}^{5+}}}\right) \tag{2.13}$$

Therefore, it is possible to deduce the state of charge during the cell operation only measuring the open circuit potential. Despite the measure is not accurate, it is widely used as first approximation because of its rapidity. Substituting Equation 2.9 and Equation 2.12 into Equation 1.8 considering the total reaction to occur in the cell, the OCP can be expressed in terms of the SOC:

$$E_{\text{cell}} = E_{\text{cell}}^{o} - \frac{RT}{nF}\ln\left(\frac{c_{\text{V}^{3+}}\, c_{\text{V}^{4+}}}{c_{\text{V}^{2+}}\, c_{\text{V}^{5+}}\, c_{\text{H}^{+}}^{2}}\right) = E_{\text{cell}}^{o} - \frac{RT}{nF}\ln\left(\frac{(1-SOC)^2}{SOC^2 \cdot c_{\text{H}^{+}}^{2}}\right) \tag{2.14}$$

The relation between the SOC and the OCP is described in Figure 2.3. It is clearly linear in the operating range of the battery but when the electrolytes are very charged or discharged there are higher gradients of potential.

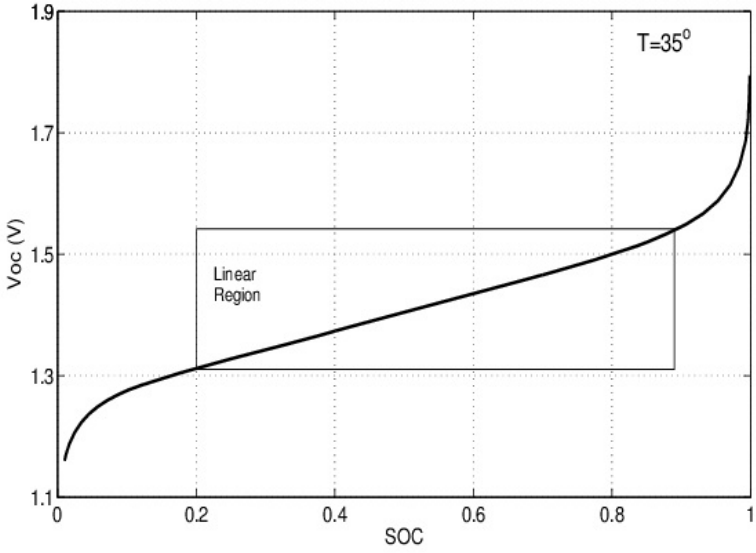

Figure 2.3: Relation between SOC and OCP [28]

2.3 Space-time and space-time yield

The space time yield measures the rate of production per unit volume of reactor and it is expressed as mol/dm h. This quantity is proportional to the effective current through the cell per unit volume of the reactor and on the concentration of the active species and the mass transport regime, current efficiency and electrode active surface area per unit volume [13]. The need to have high active surface area per unit volume of reactor is essential to achieve high current efficiency of the electrochemical reactor. In heterogeneous reactors the problem is relatively simple, but in the case of a flow battery there is the restriction for the reaction to occur the local potential must be suitable. Moreover, for the desired situation of a uniform rate of reaction over the whole electrode area the current and hence the potential must be the same all over the electrode surface.
Hence the reactor geometry is paramount concern in obtaining high surface area per unit of volume essential to a good space-time yield. Using the concept of mass balance it is possible to derive quantities useful to compare reactors and evaluate the size of the reactor for a specific production rate. The space time is defined as the time to process one reactor volume [11]:

$$\tau = \frac{c_j V_{\text{cell}}}{\dot{n}_j} \tag{2.15}$$

where c_j is the concentration of j species in the feed and $\dot{n}_j$ is the feed flow rate in molar per unit time and V is the volume of the reactor. This quantity is related to the mass transport phenomena inside the reactor. To investigate those mechanisms inside flow cell the analysis of marker experiment must be performed, but it will better explained in section 4.1.

2.4 Cost Analysis

Although the redox flow batteries are already commercialized, their costs are not yet competitive or adequate compared to other energy storage systems. A deep analysis is necessary to understand the feasibility of meeting the market targets with the actual technology and to evaluate the possible changes which might result in capital cost decrease. The cost components associated to the installation of the batteries are several: among them operation and maintenance (OM) cost, both fixed and variable, power connection system (PCS) and balance of plant (BOP) [29]. The distribution of the overall cost is illustrated in Figure 2.4.

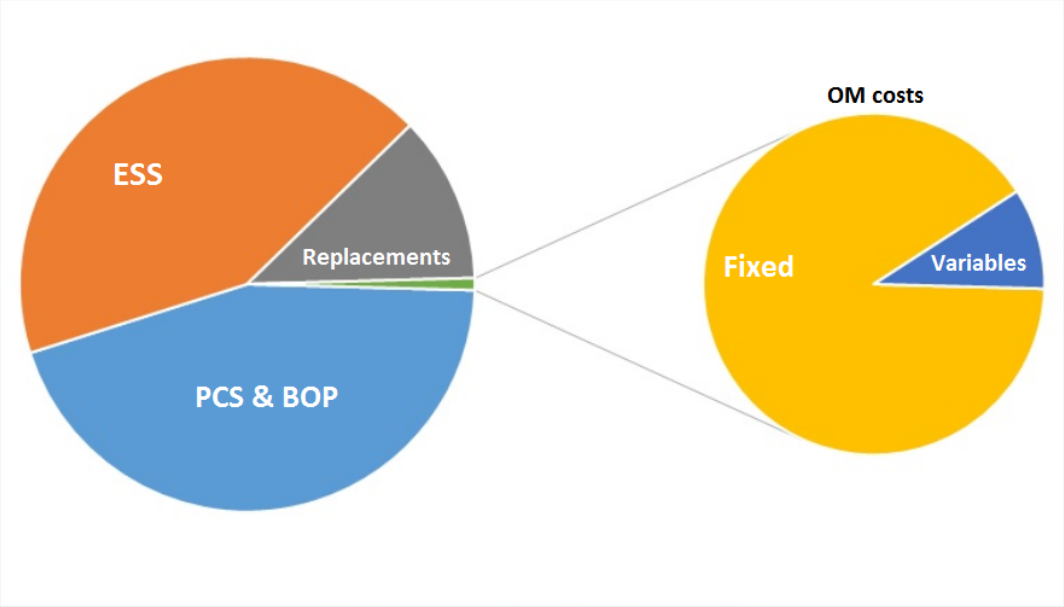

Figure 2.4: VRFB cost distribution based on [29]

In the case of the VRFB the PCS costs are the electrochemical cell and the control systems, the ESS is mainly due to the electrolytes. The PCS costs are proportional to the installed power, while the ESS is proportional to the capacity of the system. In Table 2.2, the major component of the cost of the VRFB are analyzed in detail considering the contribute of each part of the cell.

The major part of the cost is associated to the ESS part, which represents about 45% of the entire cost of the battery. The analysis assumes the source of vanadium to be V_2O_5 while the research in laboratory scale use an higher grade of vanadium $VOSO_4$, that is significantly more expensive. An interesting strategy to reduce the cost is in the production technology and materials. The intent was to decrease the capital cost to 250 US$/kWh before 2015 and another reduction up to 100 US$/kWh before 2030 [30]. So far, the results are far from the plan because the actual cost is around 400 US$/kWh [29].

Table 2.2: Internal cost of a VRFB from [29]

Cost of component	**Percentage**
V_2O_5	28
Electrolyte production	10
Tanks	7
Total storage cost	**45**
Activated carbon-felt electrode	7
Bipolar current collector	2
Frame and associated components	19
Ion-exchange membrane	2
Electrolyte storage tanks (x2)	8
Pumps (x2)	7
Control system	11
Total flow cell cost	**55**
Total capital cost	**100**

2.5 State of the art and commercialization

2.5.1 Structure and state of the art

The components used in VRFB are important to determine the life cycle and the performance of the system. The membrane must be characterized by a good chemical stability due to the high oxidizing electrolyte. Furthermore, it must have high proton permeability and electric conductivity, low permeability to the vanadium ions. The electrodes must be made of material characterized by a good electrochemical activity for the redox reaction of the vanadium and on the other hand a low electrochemical activity for the side reactions. Moreover the electrode must be chemically stable during exceptional overcharge. In the last 30 years several researches have been carried out to develop material highly performing that might also be produced with relatively low costs in order to meet the standards of the market.

Electrode

A range of electrode material have been tested and evaluated in both positive and negative half cell of VRFB. The main electrode materials can be divided into two types:

- Metals;
- Carbon;

A range of metals such as Pt, Au, Pb, platinized titanium (Pt-Ti) and iridium oxide were evaluated as positive electrodes. It was found that the electrochemical reversibility of the catholyte reaction was not sufficient in the Au electrode, while the Ti and Pt electrodes were passivated in the potential range where the reaction occurs. An increase in the electrical resistance is found because the passivation film formed in the surface. To avoid it, the use of Pt-Ti electrode is suggested but its extensive used is limited because its high cost [31].
Graphite functions well as electrode but during overcharge in the positive half cell oxygen evolution may occur and cause disintegration of the electrode surface [32]. Currently, graphite and carbon felt

are usually selected as the most suitable materials for both positive and negative electrode. Supposing the cell is protected from overcharge, a broad range of carbon and graphite felt demonstrate a high chemical and mechanical stability, even though some materials perform much better than others in VRFB. Some studies have been focused in order to improve the performance of the felt electrodes through electrochemical, chemical and thermal treatments of graphite felt and carbon felt for the purpose to enhance electrochemical activity. The modification of the electrode surface reaches great interest since the nature of the surface functional groups influences the electrocatalytic activity of this material [33, 34, 35]. In fact, the oxygen functional groups present on the carbon surface perform as active sites for many electrochemical reactions [36, 37]. The XPS showed a correlation between the increment in the activity for the vanadium redox reactions and an increase in the surface concentration of oxygen functional groups [38]. Chemical modification were also carried out in sulfuric acid, nitric acid and a mixture of both of them. The treatment consisting in hot concentrated sulfuric acid demonstrates excellent outcomes for the graphite felt, similar to the thermal treatment results [39]. Graphite felt modified with atmospheric pressure plasma jet was investigated as electrode in VRFB. The jet soak deeply through the graphite felt electrode, enhancing significantly its wettability. The energy efficiency of a VRFB using the treated electrode is affected by an improvement of 24%. Again the efficiency enhancement is due to the oxygen functional groups and the nitrogen doping introduced through the jet on the graphite surface, improving the electrochemical activity [40]. Another economical, environmental friendly and highly effective method is to apply a microwave treatment on the graphite felt. The results exhibit excellent electrocatalytic activity and reactive speed to vanadium redox reactions on a graphite sample treated for 15 minutes at 400° C [41].

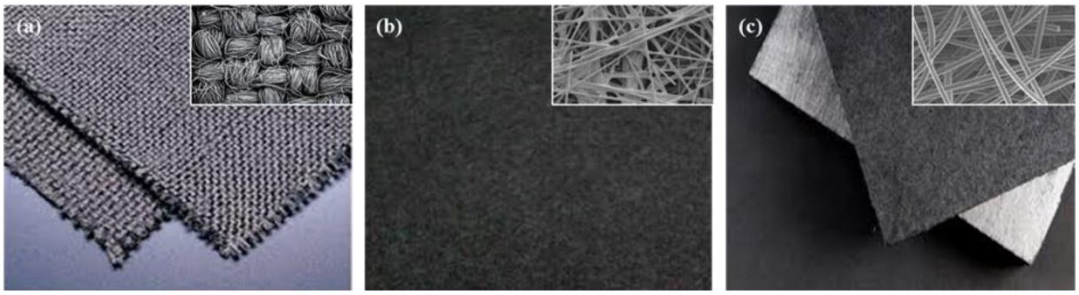

Figure 2.5: (a) Carbon cloth (b) Carbon paper and (c) Carbon felt [42]

Recently hydrothermal treatment in ammonia water was performed on carbon cloth as positive electrode with high electrochemical performances as results, showning that nitrogen doping for carbon cloth is promising for VRFB applications [43]. The effect of carbon paper on the performance of the battery was also analyzed and it shows higher electronic conductivity and electrochemical activity, facilitating the redox reactions both anode and cathode [44]. Thermal treatment in oxygen and nitrogen atmosphere of carbon paper enhance the electrochemical active area, resulting in a reduction in activation overpotential [45]. The different treatments on the electrode materials have already aimed to reduce the cost significantly but advanced catalysts both higly performing and economical must be further investigated for commercial applications. In addition to the electrochemical activity and the conductivity, the pore

structure should also be considered in electrode developing, because it can lead to a decrease in size and cost of VRFB and higher power densities [46].

Electrolyte

The electrolyte is one of the key component of the VRFB. It is the medium to store energy, and its volume and the ions concentration of the electrolyte determine the energy density of the battery.
The electrolyte consists in the supporting electrolyte and in the active species. The supporting electrolyte might be different kinds of acid such as sulfuric acid, hydrochloric acid, a mix of these or an organic electrolyte. The traditional VRFB are sulfuric acid based. The pH of the electrolyte is usually very low. The purposes of the sulfuric acid are both to provide hydrogen ions to the reaction at the positive electrode and to increase the ionic conductivity.

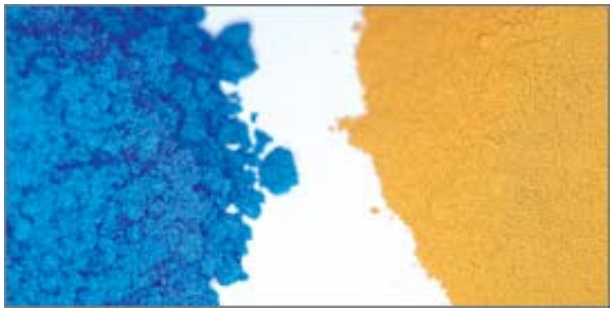

Figure 2.6: Vanadyl sulfate ($VOSO_4$) and vanadium pentoxide (V_2O_5) [47]

The active species are Vanadium ions in different oxidation states. The preparation of the electrolyte involves dissolution of $VOSO_4$ in sulfuric acid [20]. However since the high cost of $VOSO_4$ an alternative raw compound for the production became important in order to meet the market demands. V_2O_5 is a good compromise but its use in electrolyte preparation. The two different raw material for VRFB electrolytes are shown in Figure 2.6: the difference in color means the different oxidation state of the vanadium, V^{4+} for $VOSO_4$ and V^{5+} for the V_2O_5. The use of V_2O_5 is limited by its low solubility as shown in Figure 2.7.

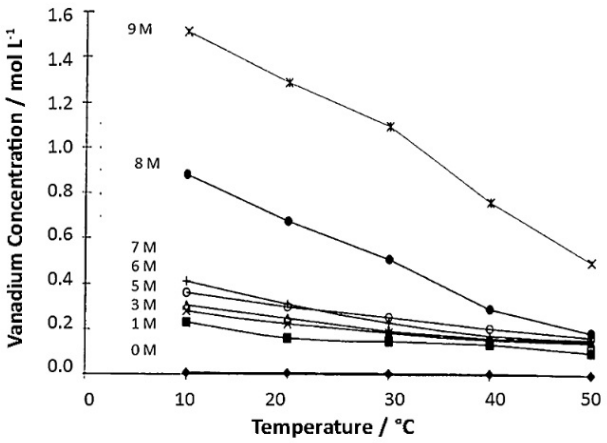

Figure 2.7: Effect of temperature on the solubility of V_2O_5 at different sulfuric acid concentrations [48]

Several vanadium compound dissolution processes were developed and this allowed the low-cost electrolyte preparation necessary for commercial implementation of the VRFB [49]. Among these processes there are the suspended powder electrolysis and the chemical dissolution using wide range of reducing agents. A different approach has been widely used by many VRFB developers is the chemical reaction dissolution of V_2O_3 combined with V_2O_5 powders in sulfuric acid [50]. The high cost of V_2O_3 and its extreme sensitivity to the oxygen makes this process economically and practically less attractive than the powder electrolysis of V_2O_5.

The concentration of active species plays an important role because an increasing in concentration will increase the energy density of the battery according to Equation 1.24.

The traditional systems based on sulfuric acid are limited by the vanadium ion solubility and stability in the electrolyte solutions over a certain temperature range, which limits the device not only in low energy density but also in very small operational temperature window. The stability of vanadium solution decreases with an increase in vanadium concentration and decrease in temperature as show in Figure 2.8 except for the V(V) which has a completely different behaviour on temperature changes as Figure 2.9.

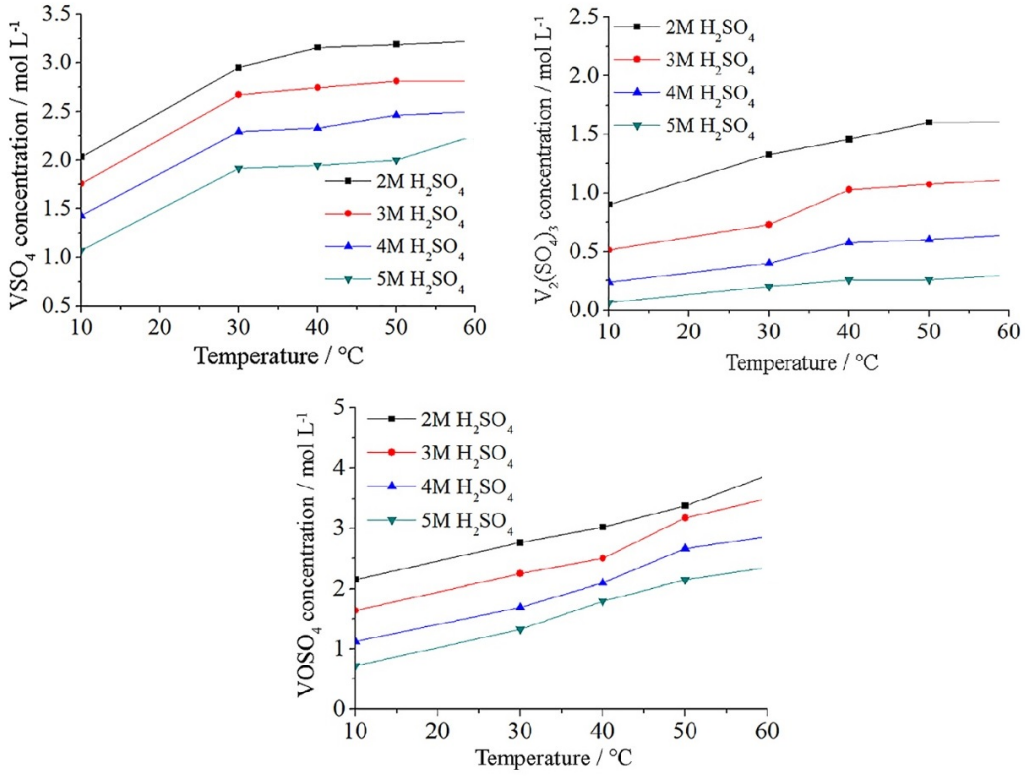

Figure 2.8: Solubility as function of temperature for different sulfuric acid concentrations from the top: V(II) and V(III) and V(IV) [49]

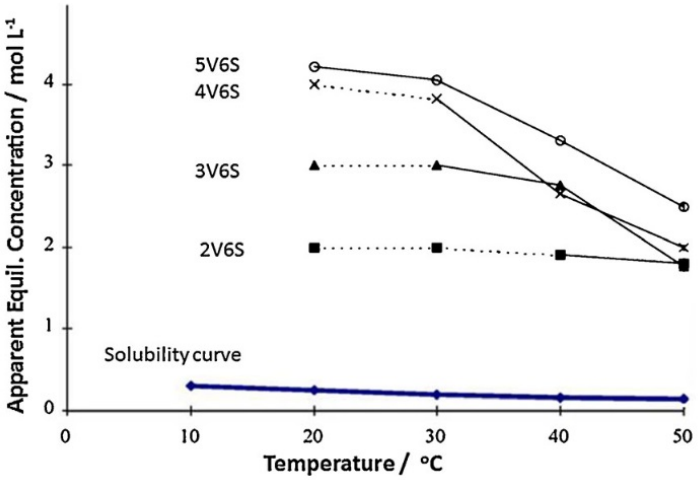

Figure 2.9: Apparent equilibrium concentration of solutions of V(V) in 6M total sulfuric acid at different temperatures [51]

Several research groups are trying to make the electrolytes more stable and to increase its electrochemical performance using additives. To achieve the objective, further advances in understanding the structure of vanadium species and their interaction with solvent ions are needed.

Membrane

The membrane is very important component of a redox flow battery because it allow to close the circuit inside the cell. In fact, the electron flow from the cathode to the anode must be balanced by a proton flow into the cell. This is possible because the membrane allow the passage of protons and it is the separator between the anolyte and catholyte to prevent mixing between them. The ideal membrane should be:

- High ion selectivity, namely low permeation rates of water and vanadium ions in order to minimize self-discharge and energy loss during charge and discharge process;
- High ion conductivity, for the transport of charge-carrying ions in order to maintain the electrical circuit close;
- Low area resistance to minimize the losses due to the ohmic overpotential;
- Good chemical stability during operation, lifetime of several years is the minimum requirement;
- Low cost, essential for worldwide application and commercialization;

The main barrier in commercialization and development of VRFB is the availability of a low-cost membrane which could meet the requirement listed above. During 1980s several commercially available membrane such as Selemion^{TM} AMV and CMV were investigated. The studies showed many of them exhibited good energy efficiency but their chemical stability in highly oxidizing environment of V(V) solution was limited and after only 2 months of working they showed significant degradation due to chemical attack [52].
Nafion has been widely accepted as optimal membrane for VRFB applications. Developed by Dupont^{TM},

this polymer contains sulfonic acid, which drives the proton-hopping form of transport. This membrane has to be hydrated to be permeable, since the hydrophilic sulfonic acid groups line up in channels ranging in size from 10 to 50 Å as shown in Figure 2.10. Through this channel pass the protons also other undesired molecule. Apart from its good proton-conductivity and chemical stability, the high cost limits the large-scale applications in the long term. Moreover, its low ion selectivity and high vanadium crossover has also limited the commercialization.

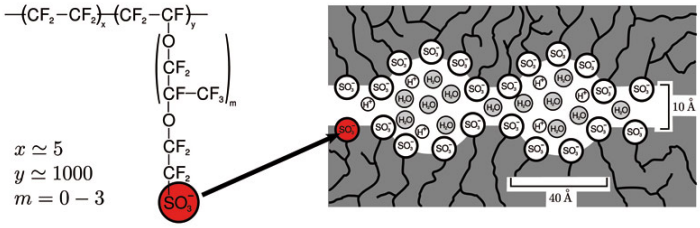

Figure 2.10: Chemical structure of hydrated Nafion membrane [53]

Another big phenomenon which must not be neglected is the water crossover, that can lead to vanadium precipitation if the concentration overcome the limits of solubility [54]. Although they do not cause irreversible damage to the battery, it is better to minimize it to not impact on the OM cost, in addition to safety reason. The problem of water transfer was widely analyzed by the pioneer team at University of New South Wales. The observations showed a net volumetric water transfer during charge-discharge cycles and it was found the direction of the transport is dependent upon the nature of the ion-selective membrane used. If membrane is employed the net transfer is toward the negative half-cell, while when is used the net transfer of water is toward the positive half-cell [55, 56]. To improve its ion selectivity, inorganic particles can be introduced into the Nafion, such as SiO_2, TiO_2 or ZrP [57, 58, 59].
Lately, the research is focusing its attention on the development of new membrane economically more attractive and more ion selective, such as not-fluorinated hydrocarbon based membranes and microporous separators [1].

Geometry

One exclusively characteristic of VRFB is that a mass flow is involved in it. Important effort has been expended to improve the mass transport of the electrolytes. In the most common setup of flow battery the electrolyte is supplied to the electrodes from the lateral side, which causes a mass transport polarization in a region far from the inlet. One possible way to minimize the mass transport losses is to increase the flow rate, but it requires an increase of the flow rate, which leads to large parasitic pumping loss. The issue can be tackled introducing a flow field through channels between the current collector and the porous electrode, which allow the flow distribution with reasonable pumping power. The importance of the flow field design has been introduced in the fuel cell state of the art [60]. Many configurations of flow field have been presented in the literature but the critical issue remain the uniform distribution of the fluid on the surface of the electrode and this usually requires a high flow rate, requiring higher pumping power which reduce the overall efficiency of the flow battery [61].

Several numerical studies have been conducted using 3D scale models in order to find the flow distribution in the channels, investigating the impact of single or multi-inlet flow rates and identifying energy and battery efficiency of different configurations [62].
A remaining important question is also how to design the cross section of the channels and how to determine its length. Small areas allow high flow rates to the electrodes, but an increase in pumping power is required. On the other hand long channels give more reaction sites but pressure losses are directly proportional to length. For this reason to maximize battery performance, channel design must take into account simultaneously the flow rate and the electrical current, since mass transport has to be balanced with electrochemical reaction rate.

2.5.2 Commercialization, applications and field trials

Despite the not competitive cost, the VRFB has already reached a good distribution and more companies are interested on the technology from the domestic application in the order of kW to the industrial application in terms of MW. One of the first appliance, based on the University of New South Wales license Thai Gypsum Products installed 5 kW-12 kWh VRFB (Figure 2.11) to support a 1 kW PV power system in Thailand. The battery was designed to store solar energy during the day so it could be used at night [63].

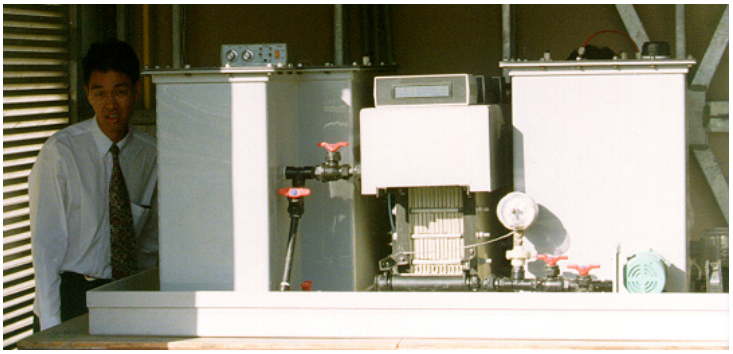

Figure 2.11: VRFB prototype installed in solar house in Thailand [64]

Another interesting application from University of New South Wales involved the installation of a 5 kW-5 kWh VRFB in a electric golf cart as shown in Figure 2.12. This test included a high energy density vanadium solution of 3M that was stabilized through additives in order to prevent precipitation under supersaturation conditions. This particular project was developed to demonstrate both electrical recharging as well as mechanical refueling, unique feature of flow batteries as shown in Figure 2.13. By exchanging discharged electrolyte, the recharge is instantaneous and the spent solution can be used as load-leveling of the grid by off-peak recharging [65].

Figure 2.12: VRFB powered electric cart [64]

During the next years, the VRFB patent was acquired by different companies which started to spread the new promising technology around the world, among them the most important are Mitsubishi Chemicals and Pinnacle VRFB.

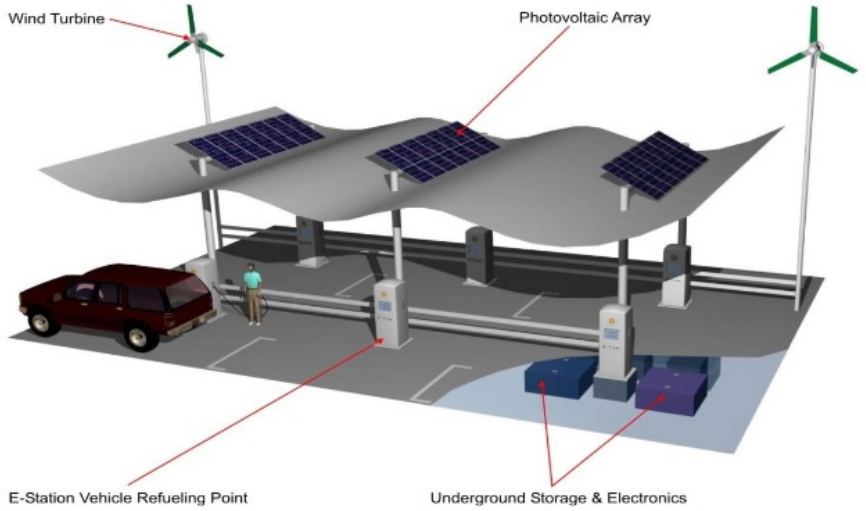

Figure 2.13: VRFB fuel station concept for electric car [66]

By 2006, the basic VRFB patent [21] had expired and so several other companies started to develop and commercialize the ESS. A selection of some application is listed in Table 2.3. The most interesting is the 200 MW installation under construction in China. The battery arrays will be made up of ten 20 MW-800 MWh VRFB ESS connected to the main grid of Liaoning province. During extreme climate events the province has experienced electric grid stress. After full commissioning, the installation will be able to peak-shave around 8% of the province's capacity in 2020. Furthermore, the large-scale battery will form an additional load center, improving the stabilization of the grid and will secure the power supply in emergency events [67].

Another interesting application is the Refrigeration warehouse project: it has the purpose to reduce the energy consumption through energy time shifting [67].

Table 2.3: Installation of VRFB for different size energy storage [67]

Project	Location	ESS Provider	Power [kW]	Year	Status
Smartregion Pellworm	Island Pellworm, Germany	Gildemeister	200	2013	Operational
PVCROPS Evora	Evora, Portugal	redT	5	2013	Operational
V.C. International airport Antigua	Antigua, Antigua and Barbuda	meeco sun2live	3 000	2015	Operational
Minami Hayakita Substation	Hokkaido, Japan	Hokkaido Electric Power	15 000	2015	Operational
Refrigeration warehouse	Icheon, South Korea	H2, Inc	67	2018	Operational
Dalian VFB	Dalian, Liaoning, China	Rongke Power	200 000	2018	Under construction

It is evident the VRFB has been proven for a wide range of application such as renewable energy storage, peak shaving, emergency backup with different rated power.

2.6 Advantages and limitations

The growing interest in VRFB is due to its several and singular advantages.

- The long lifetime of the material of the battery and the potentially endless durability of the electrolytes is a remarkable advantage compared to other batteries. Since the reaction takes place only between the electrolytes and the electrodes are the active surfaces where the reactions take places, there will not be electrodeposition or losses in the electroactive substances during the cyclic operation of the battery [17]. The lifetime of the electrolytes is dependent upon the hallmark of the VRFB that is the choice to use the same metal in both sides of the cell. Even though the membrane are very selective it is impossible to completely eliminate the crossover phenomenon. While the crossover in flow batteries with different involved metals will cause the irreversible degradation of the electrolytes, in the VRFB the only consequence is the reduction of the energy capacity, that can be restored re-balancing the solutions [68, 69]. In general it needs low maintenance in terms of investment as presented in section 2.4 and operations during the entire lifetime. Furthermore, the technology has the ability to deep discharge without affecting the cycle life [70].

- The separation between power and energy capacity is another outstanding advantage. The first is proportional to the area of the electrochemical cell, the active area of the electrodes and the number of cell stacks. The second is dependent on the volume of the electrolytes and on the concentration of active species [10]. For this reason, it allows to modify the system after the commissioning without expensive investments. Furthermore, when a flow battery is installed into a vehicle, the engine size will be related to the cell stack while the fuel tank will be represented by the electrolyte volume.

- The fast kinetic of the reactions and the significant absence of system inertia allow to reduce drastically the response time: the VRFB guarantees the frequency regulation much faster than the usual generators and support the power demand in short times, the order of milliseconds. The self-discharge is minimized since the electrolytes are stored in separated tanks, external to the

battery [71, 72].

- It has a simple SOC indicator, since the electrolytes take different colors when at equilibrium.

In spite of its potentialities, the VRFB presents also some critical issues that cannot be neglected, among them the low energy density and the high cost.

- The high cost of the electrolyte is one of the main problems related to the cost of the entire system together with the membrane as shown in section 2.4. Nevertheless, there is a possibility to obtain vanadium cheaply during the leaching of coal, in order to obtain a higher heating value of the fuel, vanadium is one of the element that can be separated [73].

- The energy density recorded for VRFB comprises values between 10 kWh/kg and 75 kWh/kg [29] and the power density does not exceed 800 MW/cm^2 [74]. Those values are relatively low compared to the traditional ESS and the reasons behind are basically the number of transferred electron of the reaction, the low OCP and the low vanadium solubility. Moreover, the vanadium solubility presents temperature boundaries as shown in section 2.5.1.

- The distribution of the solution from the tanks to the electrochemical cell must be accurately designed in order to avoid and minimize the phenomenon of the shunt currents: the presence of ions into the electrolyte make them conductive and the potential drop between the different cells of the same stack cause the formation of current from one cell to the other through the feeding channels. This currents represent a loss and it affect the overall energy produced by the battery [75]. To avoid them, it is necessary to design the electrolyte feeding system in order to alternate the inlets between the electrochemical cells or have pipes between the tanks and the stack long enough to increase the resistance and make the shunt currents negligible.

Chapter 3

Implementation

In this chapter the performed experiments will be presented, the cell is developed at the Electrochemistry laboratory, in Instituto Superior Técnico. First of all, each part of the equipment is described and progressively the construction of the cell and the preparation of the electrolyte used in the tests. Thereafter the typology of the test is explained. During this phase several parameters were changed and also the composition of the electrochemical cell, in particular sulfuric acid treatment was performed on the electrodes in order to understand the properties and features which may enhance the battery performance.

3.1 Equipment

A schematic representation of the equipment through which the experiment were performed is shown in Figure 3.1.

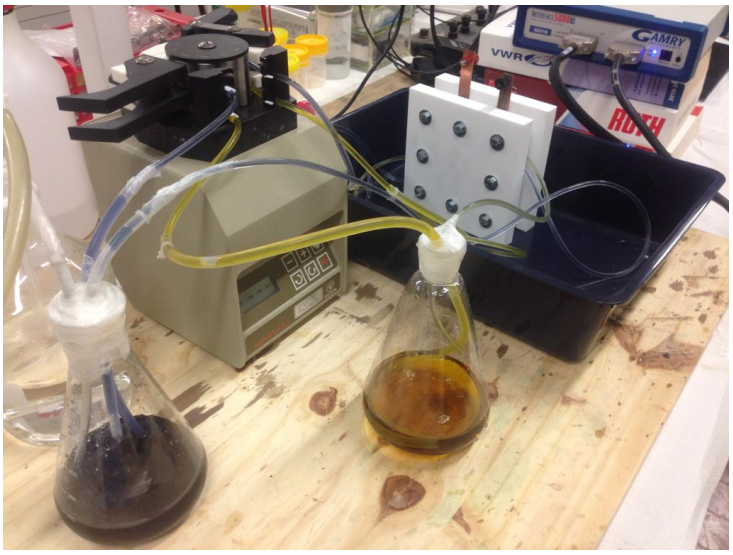

Figure 3.1: Schematic representation of the experimental equipment

The system comprises a single electrochemical cell, two tanks filled up with the electrolytes, one for the anolyte and one for the catholyte. The pipes allow the distribution of the electrolytes inside the cell

through the use of a peristaltic pump. The data acquisition device is also present in order to perform the electrochemical tests and investigate on the performance of the cell and its components.

3.1.1 Electrolytes

Two different concentration of solutions were chemically prepared. The electrolyte were produced dissolving 0.6 mol of V_2O_5 that corresponds to 109,12 g in 4 L of 6 M H_2SO_4, according to the solubility conditions in Figure 2.7, obtaining 0.3 M of vanadium ions VO_2^+. The solution was then separated in four parts of 1 L each. One part was chemically reduced to V^{2+} through Zn powder in order to have 2 L of charged solution, both anolyte and catholyte with a concentration of 0.3 M of vanadium. The rest was diluted to reach half the concentrations, namely 0.15 M of vanadium ions in 3 M of sulfuric acid to start the tests with a less aggressive solution. In order to prevent oxidation of the anolyte by atmospheric oxygen, nitrogen was supplied inside the negative tanks continuously. The electrolytes are stored in plastic tanks. Two hundred milliliters are tested for the 0.15 M of vanadium ions and for the 0.3 M concentration. The samples of electrolyte with different colors are shown in Figure 3.2.

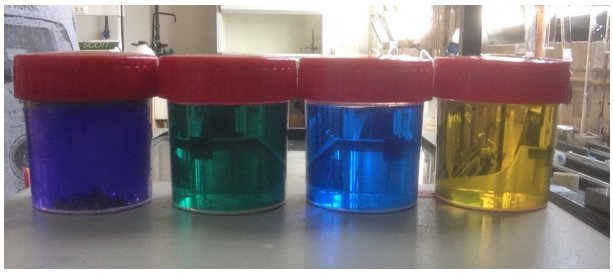

Figure 3.2: Different vanadium oxidation state distinguished by colors: from left to right V(II), V(III), V(IV), V(V)

3.1.2 Electrochemical flow cell

The objective of the work is to optimize a lab scale VRFB and study its performance in different working conditions. The electrochemical cell does not have a flow path, so the electrolytes are pumped in from the bottom of the cell and the outlets are placed on the top to ensure the filling.

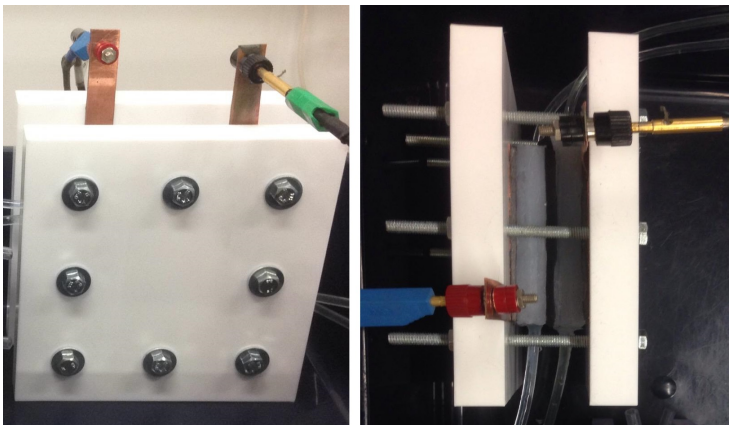

Figure 3.3: Redox flow cell: front view (left) and side view (right)

Frame, current collector and sealing

The frame of the electrochemical cell is made of PTFE 150x150 mm and 20 mm thickness. The current collectors are made of polymeric graphite and copper. The sealing consists of silicon gaskets 4 mm thickness in the outer part while EPDM gaskets 6 mm thickness in contact with the membrane.

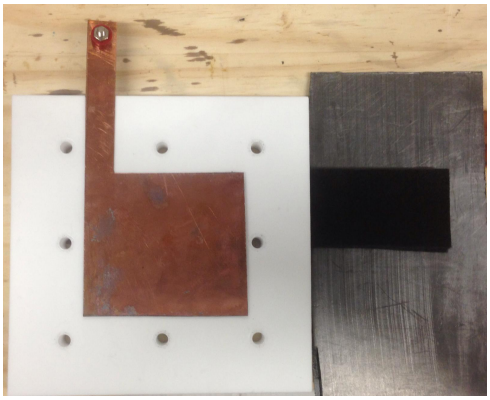

Figure 3.4: PTFE frame and copper current collector (left) and polymeric graphite and carbon felt (right)

Electrodes

The electrodes are NATIONAL^{TM} Carbon Felt grade VGD 10 mm of thickness. Its main feature is the greatly reduced gas evolution and higher oxidation resistance than standard carbon grades. The carbon felt used is 50x50 mm. The electrochemical cell was tested with the non-treated electrodes and with the acid treated electrodes thereafter. The graphite felt was treated in pure sulfuric acid at 120°C for 5h according to [76].

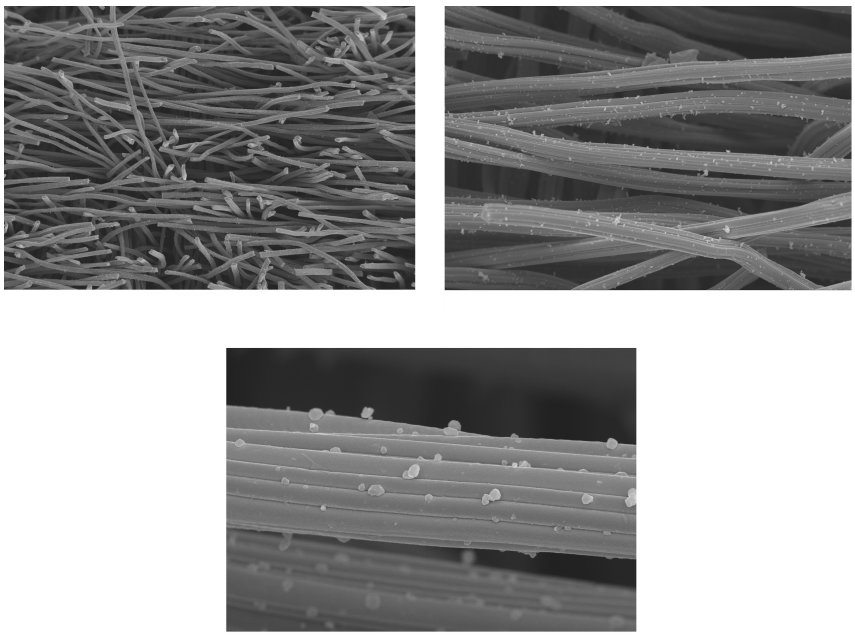

Figure 3.5: SEM pictures of the non-treated electrode NATIONAL^{TM} Carbon Felt VGD of 100x 500x and 3000x magnitudes

Membrane

NAFION®117 by Dupont™ is used as membrane to separate the anode and the cathode compartment. The membrane is non-reinforced films based on chemically stabilized perfluorosulfonic acid/PTFE copolymer in the acid (H^+) form. The polymer is chemically resistant and durable. Nominal thickness is 183 μm at dry state. Prior to use, hydration of the membrane was made boiling it in 3% w/v hydrogen peroxide for a hour in order to remove all the impurities. Then it was slightly boiled in sulfuric acid for 2 hours at 80°C in order to increase the amount of protonated sulfonic acid groups to enhance the overall ionic exchange ability of the membrane. After the activation the membrane must stay soaked in distilled water and never get dry.

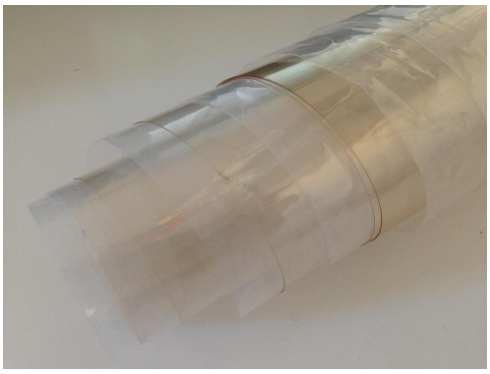

Figure 3.6: Dry NAFION®117 membrane

3.1.3 Peristaltic pump

The peristaltic pump which allows to flow the electrolytes in both sides is a GILSON™ Minipuls 3. It has interchangeable heads for delivering smooth, low pulse flows of biological and chemical fluids in 1, 2, 4, or 8 channel standard flow rate and 2 or 4 channel high flow rate configurations. It combines microprocessor speed control with a high-torque stepper motor, delivering high resolution and precision speed and control for smooth flows without sample shearing or degradation.

3.1.4 Piping system

The pipes used to distribute the flow inside the electrochemical cell are made of silicon. Two different materials were tested, in order to understand their chemical stability and their resistance to mechanical stresses, silicon and PVC, both transparent in order to see the change in color from one oxidation state to the other. The PVC tubes of 2 mm of internal diameter. The silicon tubes exhibit a bad resistance to mechanical stresses and to the acid, so in the end the PVC tubes were chosen to run the tests.

3.1.5 Potentiostat

The test were performed using GAMRY™ Interface 5000E. It can apply potential correspondent to ±6 V and the supported current is ± 5 A. The electrochemical impedance spectroscopy (EIS) frequencies goes

from 1 μHz to 1 MHz. The GAMRY^{TM} Reference 600+ was used only to perform EIS because of wider frequency range, namely from 10 μHz to 5 MHz.

3.2 Testing conditions

The research is based upon:

- Marker experiment
- Polarization curves
- Charge and discharge cycles
- Auto-discharge curve
- Electrochemical Impedance Spectroscopy (EIS)

All the experiment were carried out at room temperature. The recorded data were processed with Microsoft^{TM} Excel and the EIS spectra and the equivalent circuit with ZView^{TM}.

3.2.1 Marker experiment

The evaluation of the residence time inside the cell was essential to perform the experiments, in order to not have influence between a test and the successive one. The cell was filled continuously with the anolyte to one side and with sulfuric acid on the other side, with no current flowing at the lowest flow rate of 2.5 mL/min.

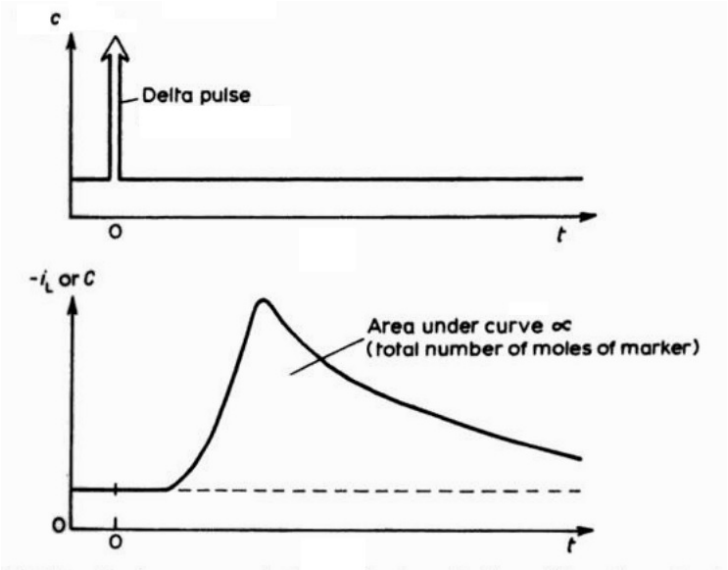

Figure 3.7: Electrochemical response of the marker experiment [11]

The marker solution consisted on 10 mL with 0.15 M concentration of V^{5+} ions. The residence time was measured injecting the marker solution the side where sulfuric acid was flowing and recording the current response of the cell. When the marker was injected a peak in the current density plot as a function

of time and a slow reduction due to the exit of the active species from the cell is evident as shown in Figure 3.7. The analysis of the response gives information about the flow conditions in the cell.

3.2.2 Polarization curves

The polarization curves are useful to analyze the generic loss of an electrochemical cell and if coupled with electrochemical impedance spectroscopy (EIS), they can give a specific interpretation of the limits on the performance of the battery [77]. The test were performed during discharging and so the imposed potential was decreasing while the supplied current was recorded. It started from a potential less than the OCP until the limiting current due to mass transport effects was reached. The tests were performed at different scan rates. Between two tests, the cell was let run for the residence time in order to have active solutions and avoid stagnation. The OCP was recorded between consecutive tests and the cell was charged when the OCP decreased more than 10 mV compared to the charge state. The performance curves were recorded at different value of flow rate, namely 2.5 mL/min, 5 mL/min, 10 mL/min and 16 mL/min. The values of the flow rate were chosen according to the rotational velocity range of the peristaltic pump in order to obtain a uniform variation between each flow rate. The polarization curves were used as tool of assess for the acid treatment performed in the electrodes. Then the tests were performed with the most efficient electrode with electrolyte of double of the concentration.
The polarization curve plot shows the available potential of the electrochemical cell associated to a specific current density and it shows the behave with several operating conditions. The plot points out the main causes of loss as in Figure 3.8.

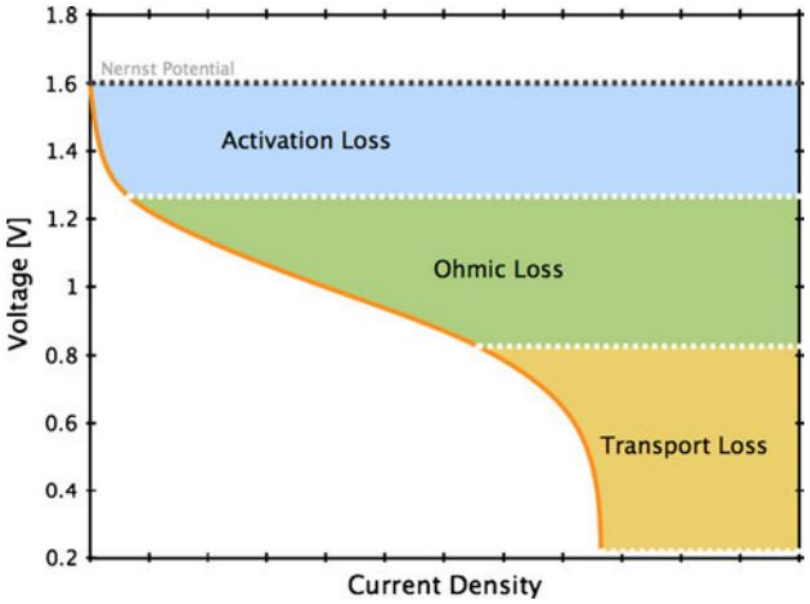

Figure 3.8: Generic polarization curve [77]

3.2.3 Charge and Discharge cycles

The objective of the charge and discharge cycles test is to obtain information upon the time stability and the working efficiency of the battery. The volume of the electrolytes was limited just on the amount inside the cell and without the use of the pump. The tests cannot replace a more complete dynamic tests where the solution are circulating and there is a progressive decrease in the state of charge of the tanks. Nevertheless, these type of tests are enough to understand the performance of the battery in short times [78].

The solution were charged at constant current of 100 mA until the potential value of 1.7 V in order to avoid high overpotential that can cause side reaction such as hydrogen evolution in the the anolyte compartment [79] and graphite corrosion in the catholyte compartment [80]. The same current intensity value was used to discharge the electrochemical cell.

The test were performed for the acid treated electrodes and the non-treated electrodes, and the electrolytes with the two different concentrations were also evaluated.

3.2.4 Self-discharge behaviour

The self-discharge tests aim to determine the viability of the electrolytes and the membrane permeability to active species. The tests were performed without flow, to reproduce the real application of the battery during its rest time. The test aims to evaluate the self-discharge for the electrolyte inside the cell and the permeability of the membrane to the active species that might cause self-discharge. In particular, the reactions induced by vanadium ions crossover are [81]:

Positive half-cell

$$V^{2+} + 2\,VO_2^+ + 2\,H^+ \longrightarrow 3\,VO^{2+} + H_2O$$

$$V^{3+} + VO_2^+ \longrightarrow 2\,VO^{2+}$$

Negative half-cell

$$V^{2+} + VO_{2+} + 2\,H^+ \longrightarrow 2\,V^{3+} + H_2O$$

$$2\,V^{2+} + VO_2^+ + 4\,H^+ \longrightarrow 3\,V^{3+} + 2\,H_2O$$

The test were performed with a prior charge made galvanostatically at 100 mA for the charge time evaluated in the charge-discharge cycles and then the OCP was recorded in function of time. The test were performed and the self-discharge was tested for the two different concentration of active species in the electrolytes.

3.2.5 Electrochemical Impedance Spectroscopy (EIS)

The EIS can be performed in galvanostatic mode or potentiostatic mode. The galvanostatic mode was chosen to perform the experiments because in a low-impedance device such as supercapacitor or battery, the application of a 10 mV sine wave produces amperes of current-flow, possibly changing the state of the device or damaging it. The EIS records the response of the device to a sinusoidal signal of potential applied of fixed amplitude and decreasing frequency. The response of the system will be a current signal

which will be characterized by a phase shift and damping. This allow to create an equivalent circuit which represent the internal resistance of the device at the different frequencies applied. The Nyquist diagram plots the impedance as imaginary and real part while Bode diagram as phase and frequency [82]. At each frequency different phenomena take place. At high frequencies the kinetic effects while at low frequencies the mass transport effects. Through the EIS the phenomena can be distinguished, but since the VRFB works with liquid electrolytes it requires frequencies lower than 0.1 Hz [83].

The range of small frequencies field was not studied in this work because of dispersion and to minimize the time evolution of the system. The EIS was run between the 100 kHz and 100 mHz with a step decay of 10. The signal was chosen by the potentiostat. The EIS was carried out with electrolyte flow at 16 mL/min for the different concentration of vanadium in the electrolytes. After the first run the influence of the membrane in the internal resistance of the cell was evaluated, performing an EIS with two membranes.

Chapter 4

Results

In this chapter the results of the tests for the chosen treatment different working condition will be presented.
The result from the marker experiment will be presented for the lowest flow rate, in order to understand the space-time for the electrochemical reactor and be sure each test will not be affected by the previous ones. Polarization curves at different scan rates and flow rates were carried out for the non-treated graphite felt electrode and the one treated with acid. Charge-discharge cycles were performed without electrolytes flow for both electrodes and using the electrolytes with double of concentration for the most efficient electrodes. The self-discharge plot was performed with the most efficient electrode as well since the phenomenon is dependent on the membrane permeability and on the electrolytes.
Polarization curves, charge-discharge cycles, self-discharge and EIS were repeated for a more concentrated solution with the electrode that resulted the most efficient thereafter.

4.1 Marker experiment

The current and charge responses to the marker injection as function of time are shown in Figure 4.1. The injection was done at 150 s after the current was stable for 1 minute. Although the geometry of the cell does not ensure the complete recirculation of the marker due to possible stagnation points, it is assumed the space-time is reached when the current is stable for one minute at 15% of the current peak. The current peak corresponds to 0,07 A and the time for the current to stabilize at 0,03 A is around 550 s. The space-time is dependent upon the geometry of the cell as explained in section 2.3, so it will not change for the other half-cell, but the peak current might have changed if the other half-cell was tested. There is a high distribution of space-time yield proven by the high peak. The half of the species contained in the marker was converted in the first 100 s.

The marker experiment was also used to estimate the efficiency of conversion of the electrochemical cell. The amount of active species injected corresponds to:

$$Q_{av} = VcF \tag{4.1}$$

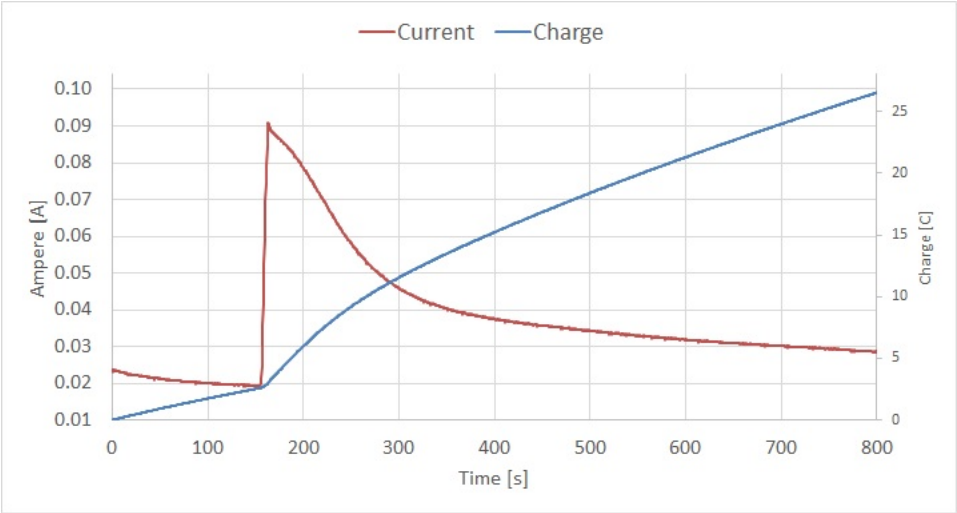

Figure 4.1: Current and charge response to the marker experiment at 150 s

Since the integral of the current over the time corresponds to the charge, the area below the current peak correspond to the amount of active species actually converted, in particular:

$$Q_{conv} = \int_{150}^{800} \Big(i(t) - i_0 \Big) dt - \int_{0}^{150} i(t) dt \tag{4.2}$$

Where i_0 is the value of the current before the injection, 20 mA. The conversion efficiency is defined as:

$$\eta_{conv} = \frac{Q_{conv}}{Q_{inj}} = \frac{i\, A_e}{F\, c\, \dot{Q}} \tag{4.3}$$

And in this case the reaction rate corresponds to 10%.

4.2 Scan rate influence on polarization behaviour

The effect of the scan rate on the polarization behaviour of the cell has been investigated in order to choose the scan rate at which perform the experiments. As shown in Figure 4.2 the total current increases with the scan rate.

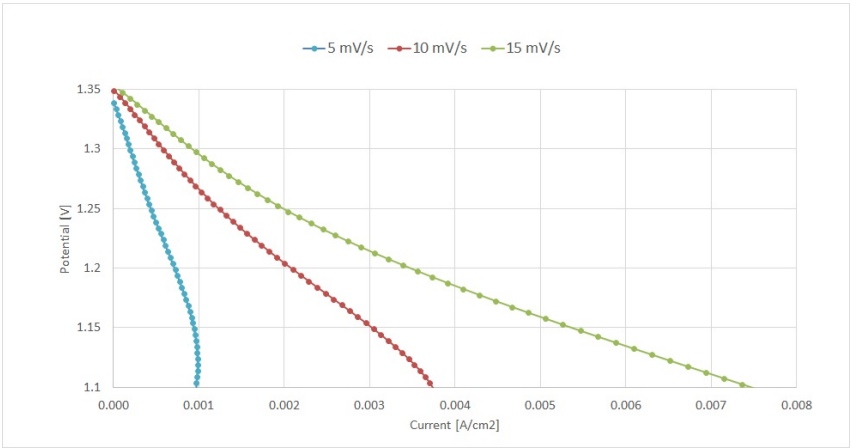

Figure 4.2: Effect of the scan rate polarization curves

As the scan rate changes the thickness of the diffusion layer above the electrode surface will be different and it will depend upon the scan rate used. In particular, in the case of slow scan rates, the diffusion layer is very thick while at faster scan rates the diffusion layer is relatively thinner. Consequently the flux to the electrode surface is higher at fast scan rates than it is at slower scan rates. Since the current is proportional to the flux to the electrode the magnitude of the current will be lower at slow scan rates and higher at fast scan rates [14].

The slowest scan-rate test was performed at the end it exhibits a different in OCP of 10 mV due to the effect of the previous polarizations. The activation overpotential is observed to increase with the the scan rate. The ohmic region is evident at all the scan rate, characterized by a reduction in the resistance while the scan rate increases. The mass transport effect is observed only at the slowest scan rate because fast curves are very much away from the real working conditions, i.e. steady state and the system does not have time for relaxation. The longer measurement periods with lower scan rates resulted in higher contamination of the electrolyte causing a significant reduction in the active species and the electrolytes needed to be charged.
In order to reduce the time in which the experiments were carried out and to not compromise too much the electrolytes with the LSV tests it was chosen to use a scan-rate of 10 mV/s.
To validate the results the polarization curves were carried out three times at the same conditions let the electrolytes circulating at the maximum flow rate of 16 mL/min between each test for the space-time evaluated in section 4.1 and the results were consistent. The maximum evolution of the system as a result of the consecutive polarization corresponds to 20% and it was always recorded at the lower scan rate. As shown in Figure 4.3 the higher deviation always come up between the first test and the second, probably because the mass distribution inside the cell was still affected by the recirculation at maximum velocity. This lead to a slow decrease of the current density in every test carried out at different conditions.

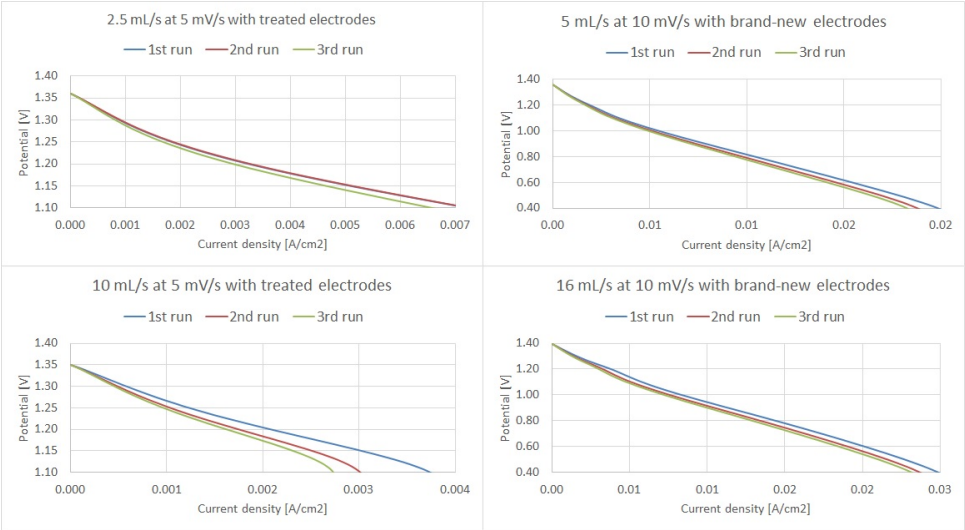

Figure 4.3: Example of consecutive tests at different conditions

4.3 Polarization behaviour

The polarization curves were carried out in the electrochemical cell varying one parameter each time, to see the influence in the overall performance of the battery. For these tests a potential scan rate of 10 mV/s was used.

4.3.1 Flow rate influence

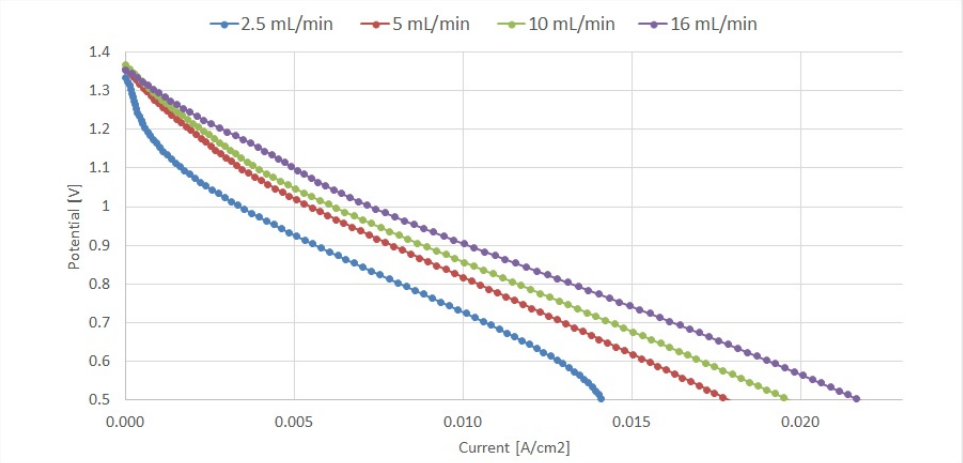

Figure 4.4: Polarization curves at different flow rates with non-treated electrodes at scan rate of 10 mV/s

Figure 4.4 shows an linear increase in current density with an increase in the flow rate, the trend is shown in Figure 4.5 at potential of 0.7 V.

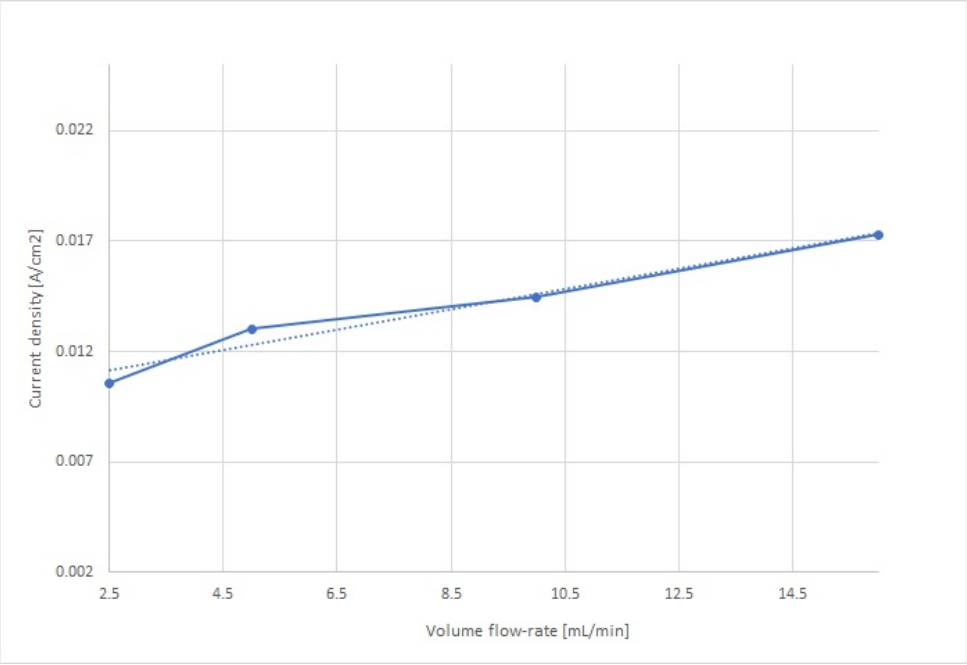

Figure 4.5: Trend of current as a function of the flow rate at 0.7 V

There is a relevant increment between 2.5 mL/min and 5 mL/min and it is probably because of a more uniform distribution of the electrolyte inside the cell and the increase of the turbulence avoided

stagnation points which may cause a decrease in current density. For higher velocities the mean increase among them is 16%. It is evident that at low flow rates both activation overpotential and the mass transport effect are relevant already at low current densities. It can be explained because the flow rate is not sufficiently strong to ensure the replacement of the solution absorbed by the electrode with new reagents that start to be insufficient, also because of the very deep weft of the carbon felt. The ohmic linear part shows an improvement with the increase of the flow rate, which lead to an increase of the power of the cell. The maximum amount of current intensity was 250 mA at 16 mL/min. The range of maximum power supplied by the cell in these conditions are 7 mW/cm^2 and 12 mW/cm^2.

4.3.2 Acid treatment influence

The influence of the flow rate was then investigated for the acid treated electrodes and then compared with the results obtained for the non-treated electrodes.

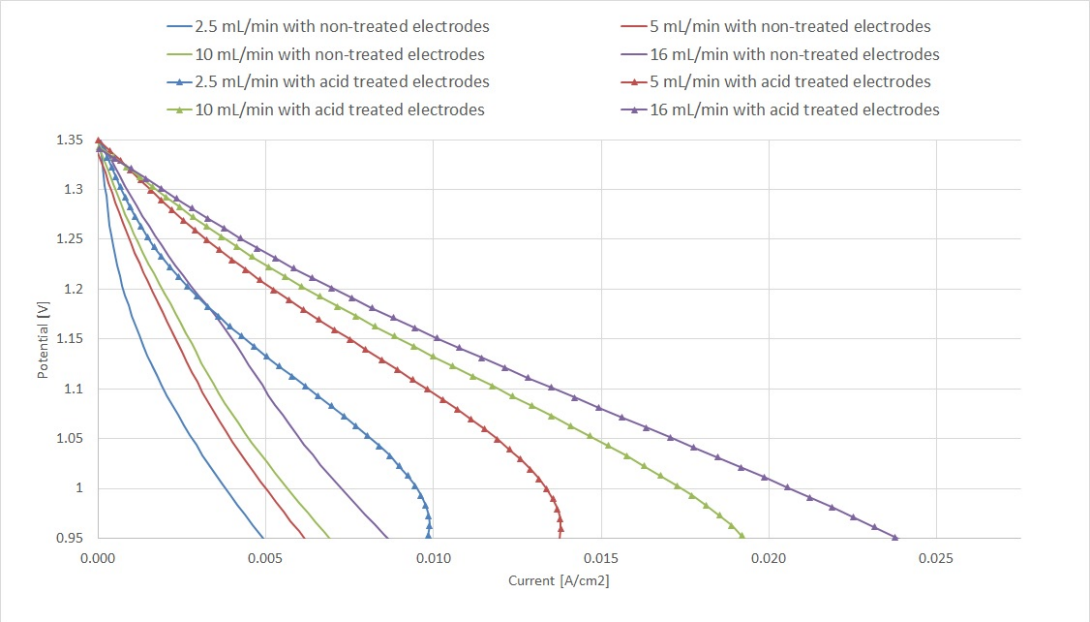

Figure 4.6: Polarization curves at different flow rates with non-treated electrodes and acid treated electrodes at scan rate of 10 mV/s

As shown in Figure 4.6 the acid treatment on the electrodes exhibits an overall increment in current density. The lower flow rate for both electrodes show a detachment from the lowest current densities, presenting an evident section due to activation losses. The influence of the flow rate in the electrodes treated with acid appears to be more significant. The higher improvement in current density can be seen from the lowest velocity to its double, which correspond to an average of 20%. Among the higher flow rates the increment in current density has an average of 40%, higher than the increase for the non-treated electrodes.

The plot for the current as a function of the flow rate at potential of 1 V is presented in Figure 4.7 and the normalized curve to the minimum value of current for the acid treated electrodes and the non-treated electrodes.

Both curves present a linear dependence between the current density and the flow rate, but the plot of

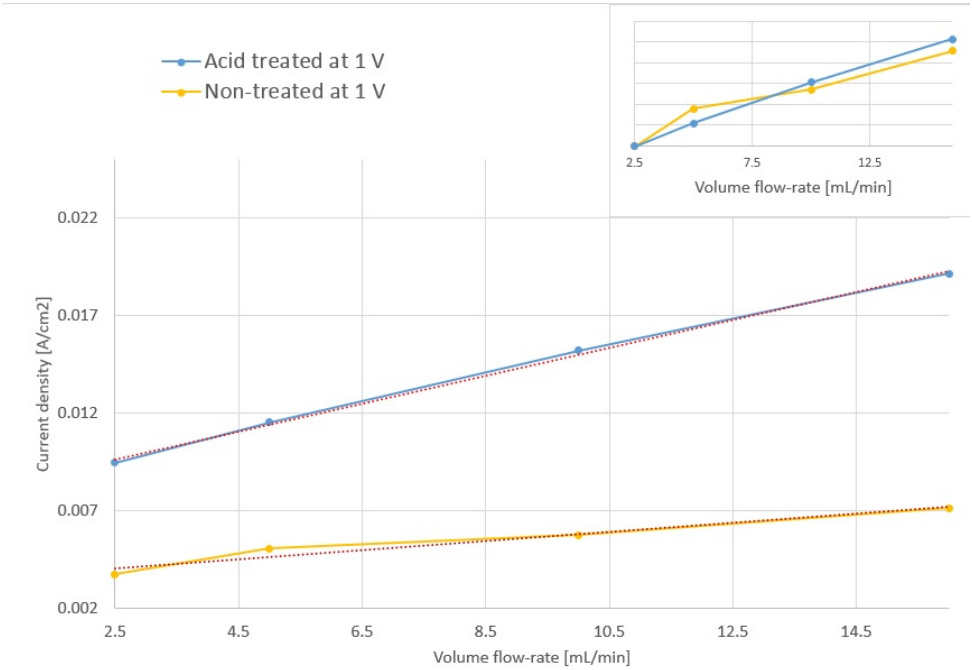

Figure 4.7: Trend of current as a function of the flow rate at 1 V for the non-treated and the acid treated graphite felts and the normalized plot

the acid treated electrodes exhibits a more uniform linear dependence. The non-treated electrode curves shows a higher improvement between the first and the second flow rate and subsequently the influence of the flow rate becomes less relevant. The values of the resistance from Figure 4.6 are listed in Table 4.1:

Table 4.1: Resistance values at different flow rate for the 0.15 M of V electrolytes with acid treated electrodes

Flow rate [mL/min]	**R [Ω·cm^2]**
2.5	35.7
5	25
10	20
16	16

The increase in the current density from the non-treated electrodes to the graphite felts treated with acid might be due to an increase in the electroactive area of the electrodes due to the acid treatment. In fact, the Figure 4.8 shows degradation of the carbon fibers. The maximum amount of current intensity recorded with the acid treated electrodes is 600 mA at 0.95 V while for the non-treated electrodes is 212 mA.

The non-treated electrodes can reach the same value of current but at lower range of potentials, so the output power is lower. In particular the range of maximum output power for the acid treated electrodes is between 10 mW/cm^2 and 23 mW/cm^2.

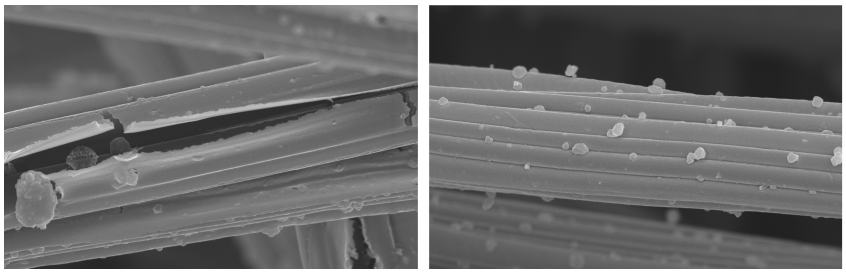

Figure 4.8: SEM image of acid treated electrodes (left) and the non-treated (right) at magnitude of 3000x

4.3.3 Concentration influence

The solutions with the double of concentration were tested as well with the electrodes treated in acid, as they have shown in the past experiments a better performance. The results for the solutions of 0.3 M of vanadium compared with the 0.15 M are presented in Figure 4.9. The values of the resistance from Figure 4.9 are reported in Table 4.2.

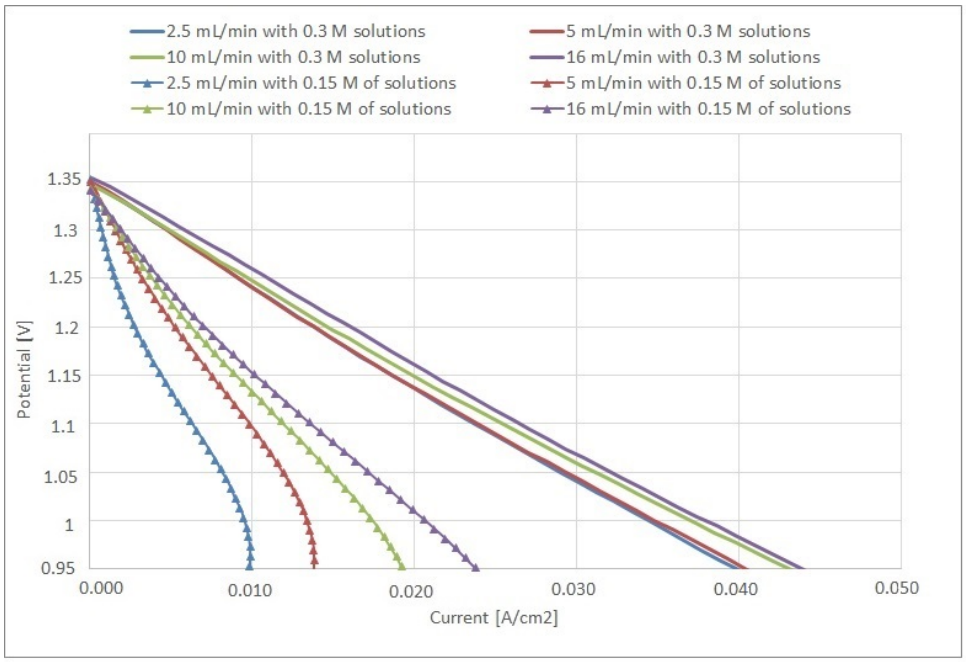

Figure 4.9: Polarization curves at different flow rates for 0.15 M and 0.3 M solutions

The polarization plots for the solution of 0.3 M do not show the same characteristic trend as the polarization curve recorded so far. The activation losses are almost negligible. The more concentrated solutions do not show a strong dependence on the flow rate and it means there is no need to high turbulence in order to distribute the solutions into the electrodes. Therefore, it is not convenient to work with high flow rates because of the power supplied to the pump. The tests are stable and does not modify its shape even presenting a long ohmic range. The increment of reagents in the electrolytes exhibits a remarkable

enhancement on the performance of the battery, with current that results the double compared to the the less concentrated solutions. While the 0.15 M solutions present a section where the concentration losses are evident in the more concentrated solutions the losses do not appear relevant. The maximum value of current intensity recorded corresponds to 1.1 A. The value of the output power are not so different between the curves since the flow rate was not a key parameter. The range of output power is between 38 kW/cm^2 and 40 kW/cm^2.

Table 4.2: Resistance values at different flow rate for 0.3 M of V solutions with acid treated electrodes

Flow rate [mL/min]	**R [Ω·cm^2]**
2.5	10
5	10
10	9.7
16	9.4

4.4 Charge-discharge cycles

The results for four consecutive charge-discharge cycles for the non-treated electrode and the electrolytes of 0.15 M of concentration are presented in Figure 4.10. It is evident that for each consecutive cycle the charge-discharge cycle time is reduced by 2% .

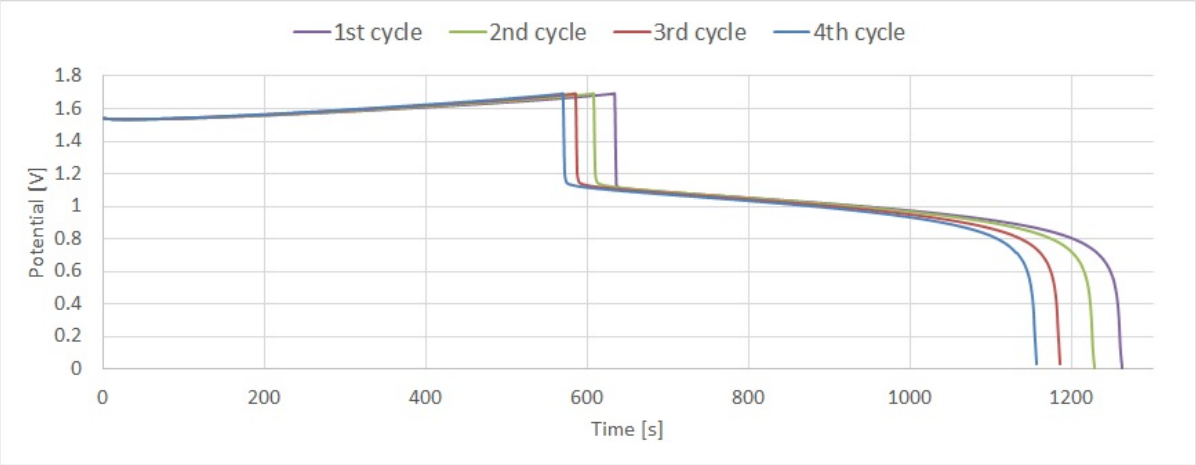

Figure 4.10: Charge-discharge cycles with non-treated electrodes

Although the reduced time of the tests, the reduction of the time of the cycle might be caused by the solution aging, which is correlated to the vanadium ion crossover through the membrane and the reaction associated to it or because of hydrogen evolution which is suppose to occur when the the potential overcome 1.6 V. Since the current efficiency of the system, according to the Equation 1.28, results to be higher than 90% for each cycle, this phenomenon is negligible. The first part of the graph corresponds to the charge phase, where the potential slowly increases until the imposed value is reached. The discharge phase begins when there is a potential drop and the slope of the curve changes, showing a linear decrease of the potential with time. According to Equation 2.14 the working potential of the cell is between 1.3 V and 0.9 V. The evident drop in potential at the end of the discharge is caused by the mass transport

effects that can be seen in some of the polarization curve in section 4.3.

4.4.1 Acid treatment influence

It is evident from Figure 4.11 that the acid treatment of the carbon felt electrodes improved the performance of cell. The time for one cycle is increased by 20%. The same behaviour is evident each time a charge-discharge cycle was performed, but with the acid treated electrode the reduction is smaller compared to the non-treated electrodes. The working potential range is higher and it affects the potential efficiency of the cell and the overall energy energy of the battery.

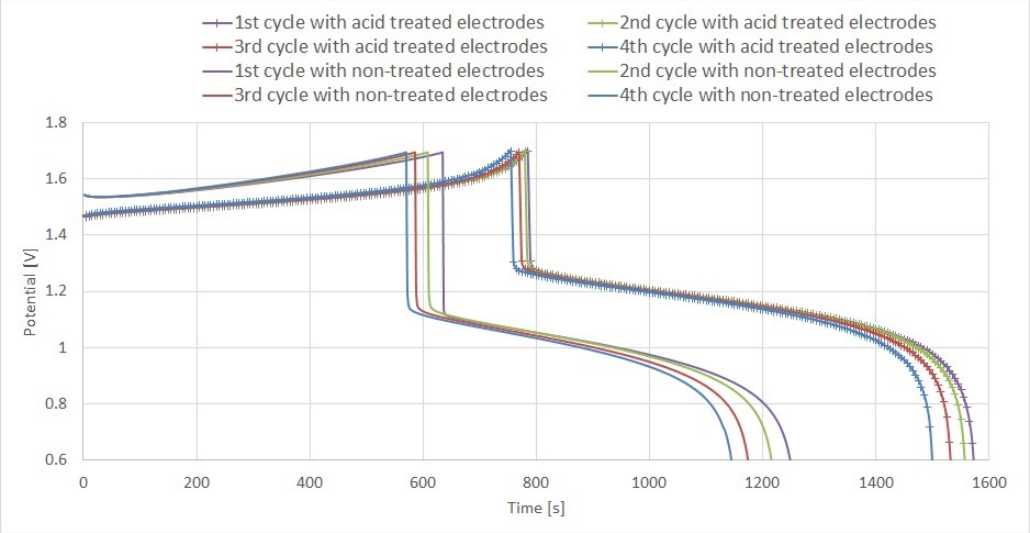

Figure 4.11: Charge-discharge cycles with non-treated electrodes and acid treated electrodes

4.4.2 Concentration influence

The outcomes of the charge-discharge cycles tests for the acid treated electrodes with 0.3 M solutions are presented in Figure 4.12.

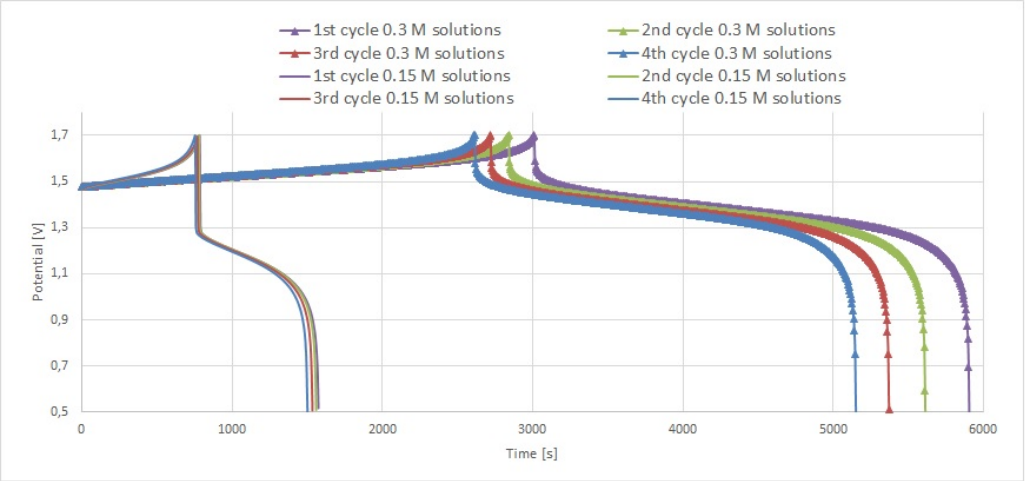

Figure 4.12: Charge-discharge cycles with 0.15 M and 0.3 M solutions

The use of the identical cell configuration and charge-discharge cycles setup and electrolytes with the double of concentration suggest the time for each cycle will be doubled. From the outcome of the experiment it is evident the time is increased of more than three times. So the use of more concentrated solution enhance the performance of the battery. The reduction of the time for each cycle is reported, the same of the less concentrated solutions. There is an evident increment in the working potentials during the discharge and this is because the more concentrated is the solution the higher will be the voltage according to Equation 2.14. This affects the potential efficiency as well as the energy efficiency.

According to Equations (1.28), (1.29) and (1.30) the average values for each modification are listed in Table 4.3.

Table 4.3: Average value of current, potential and energy efficiency

	Current efficiency [%]	**Potential efficiency** [%]	**Energy efficiency** [%]
Non-treated electrodes 0.15 M of V	98.01	68.5	60.28
Acid treated electrodes 0.15 M of V	99.51	74.33	73.97
Acid treated electrodes 0.3 M of V	93.15	87.41	81.42

The influence of the cycles on the efficiency for the different electrodes and for the different solutions are presented in Figure 4.13. The reduction is less than 1%, except for the voltage efficiency between the first cycle and the second with the acid treated electrodes.

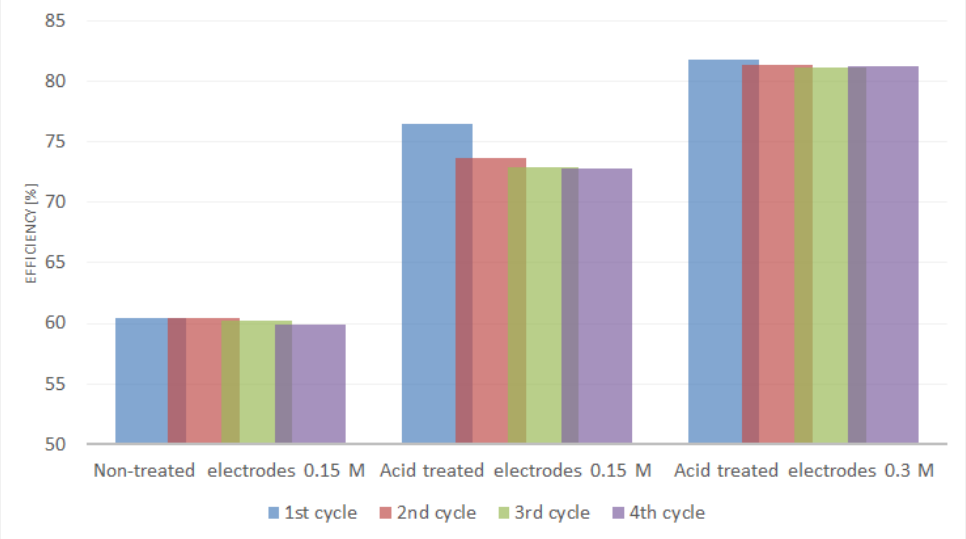

Figure 4.13: Effect of consecutive tests on energy efficiency for different setups of the cell

The influence of the modification on the electrochemical cell on the different efficiency values are presented in Figure 4.14.

The treatment shows an improvement in the coulombic efficiency as well as in the potential efficiency and energy efficiency. The increase in the concentrations exhibits a decrease in current efficiency but an increase in voltage efficiency as expected and in the energy efficiency of the battery.

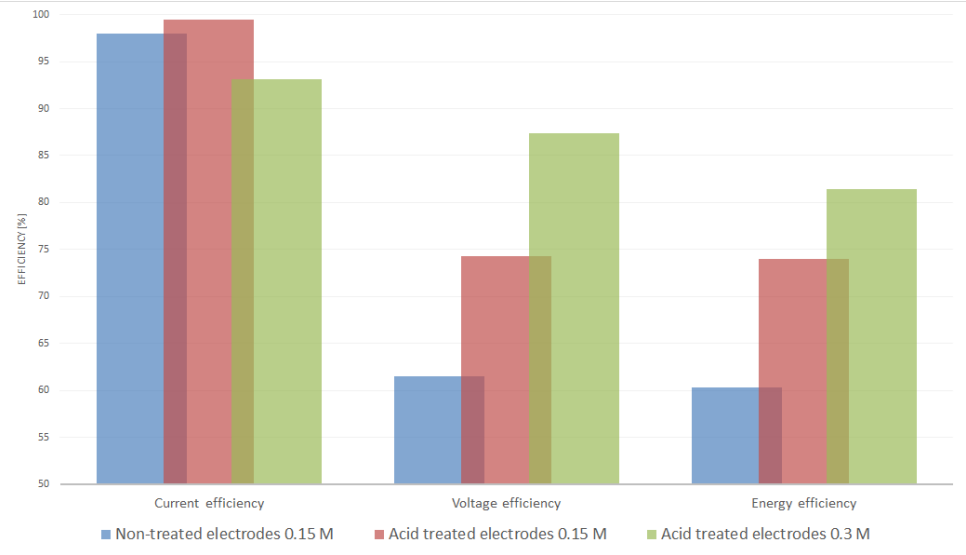

Figure 4.14: Values of efficiency for different cell setups

4.5 Concentration influence on the self-discharge

The self-discharge results are shown in Figure 4.15 together with a normalized curve to see each trend.

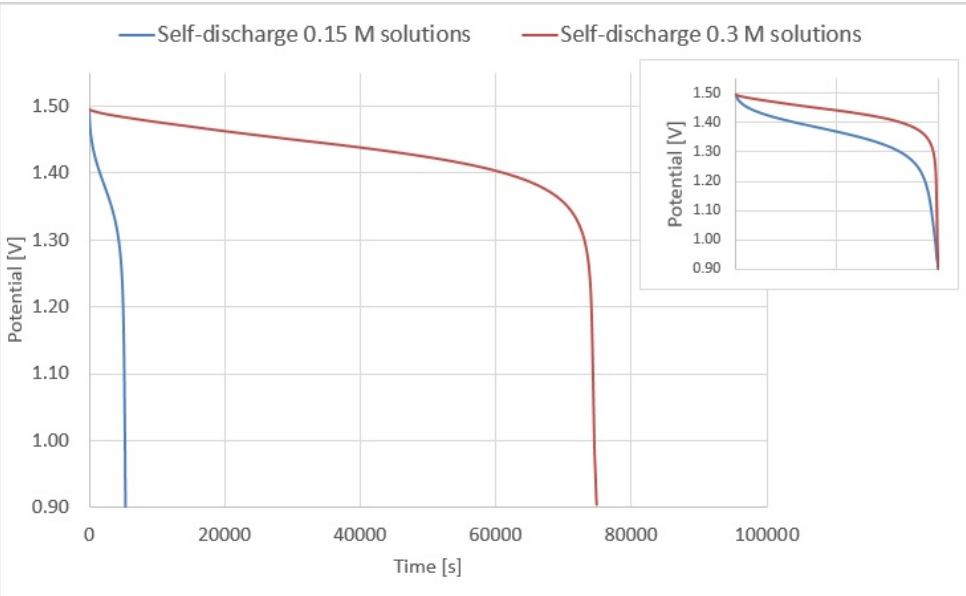

Figure 4.15: Self discharge curve for 0.15 M and 0.3 M solutions and self discharge curves normalized to the time (corner)

It could be expected that the membrane was more permeable to the solutions with more active species, but apparently the 0.3 M of V solutions took about fifteen times more time to self-discharge than the less concentrated electrolytes. The delay in self-discharging with the increase in concentration might be due to the difference in the viscosity of the solutions since the concentration was doubled for the vanadium as well as for the sulfuric acid. The difference in the trends is because the concentration affects the OCP and consequently the value for the 0.15 M electrolytes results lower.

4.6 EIS measurements

The Nyquist plots are characterized by two capacitive loops, plus an ohmic resistance corresponding to the high frequency interception of the real axis. The ohmic resistance is related to the electronic transport, the electrolytes and the resistance to ionic conduction. The semicircles characterize a resistance-capacitance behaviour, usually associated to the electrode/electrolyte double layer, the transfer of active species or the mass transport effects. The time constant were read from the Bode plots.

Under spontaneous conditions, steady state was not attained in the initial 45 minutes of discharge. Figure 4.16 shows an increment of the area underneath the semicircle in subsequent spectra revealing that steady state was not achieved for at least 45 minutes of cell working time.

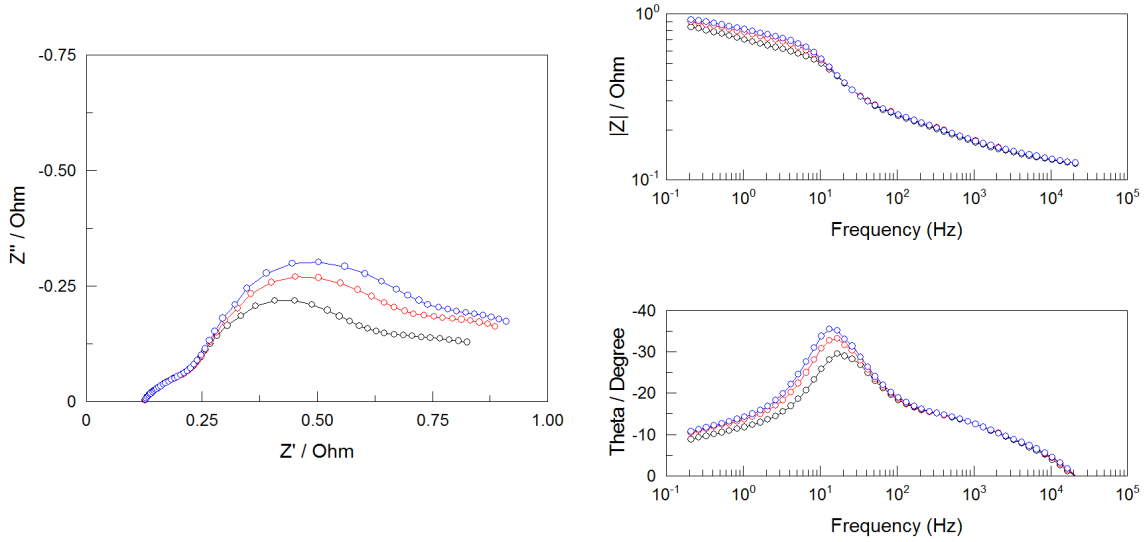

Figure 4.16: First run of EIS (black), second run of EIS (red) and third run of EIS (blue)

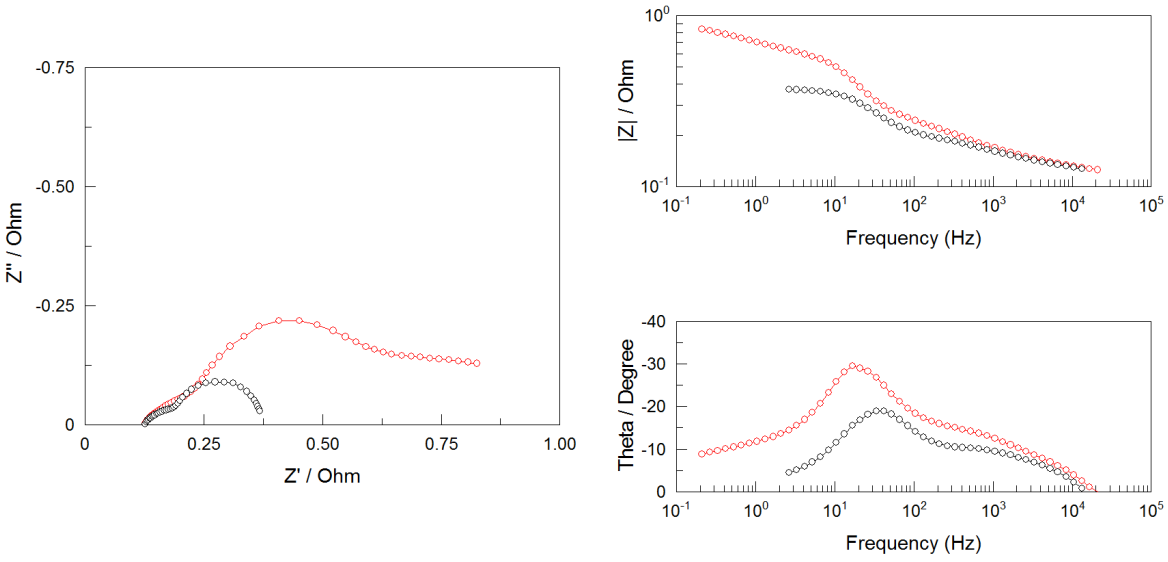

Figure 4.17: Influence of active species concentration on EIS: 0.15 M of V (red) and 0.3 M of V (black)

Figure 4.17 which presents the influence of the concentration on the EIS shows the low frequency capacitive loop has higher resistance for the curve with lower concentration. This is probably because the presence of more active species in the solutions leads to an increase in the current and consequently a decrease in the total resistance of the cell.

The effect of the membrane on the spectra was investigated by making an experiment in which two membrane were mounted in series. From Figure 4.18 it is evident that the membrane contributes only to the ohmic resistance, it does not accumulate charge. The ohmic resistance went through a two-fold increase, which means that the resistance of the membrane is approximately 0.125 Ω and since the area is 25 cm^2 the specific resistance of the membrane will result to be 3.125 Ω/cm^2.

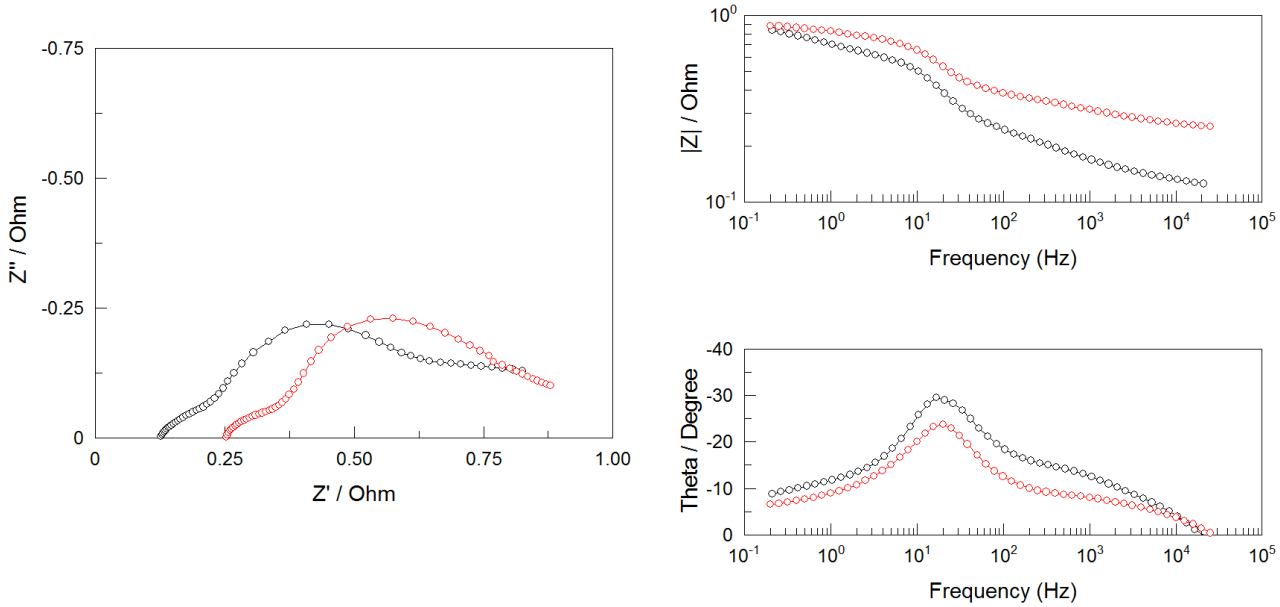

Figure 4.18: Impedance of a cell mounted with a single membrane (black) and with folded membrane (red)

4.6.1 Electrochemical modelling of the cell

The spectra were analyzed using the equivalent circuit (EC) approach. The EC is build for the curve at different concentrations. The EC and the spectra with the respective fittings are shown in Figure 4.19.

Table 4.4: Value for the component of the EC

Element of the EC	**Value**	
	0.15 M of V	**0.3 M of V**
R0 [$\Omega \cdot cm^2$]	3.11	3.18
CPE1-Q_0 [$F \cdot s^{n-1}/cm^2$]	0.0021	0.0010
CPE1-n	0.647	0.745
R1 [$\Omega \cdot cm^2$]	3.59	1.83
C2 [F/cm^2]	0.00153	0.0016
R2 [$\Omega \cdot cm^2$]	10.18	4.31

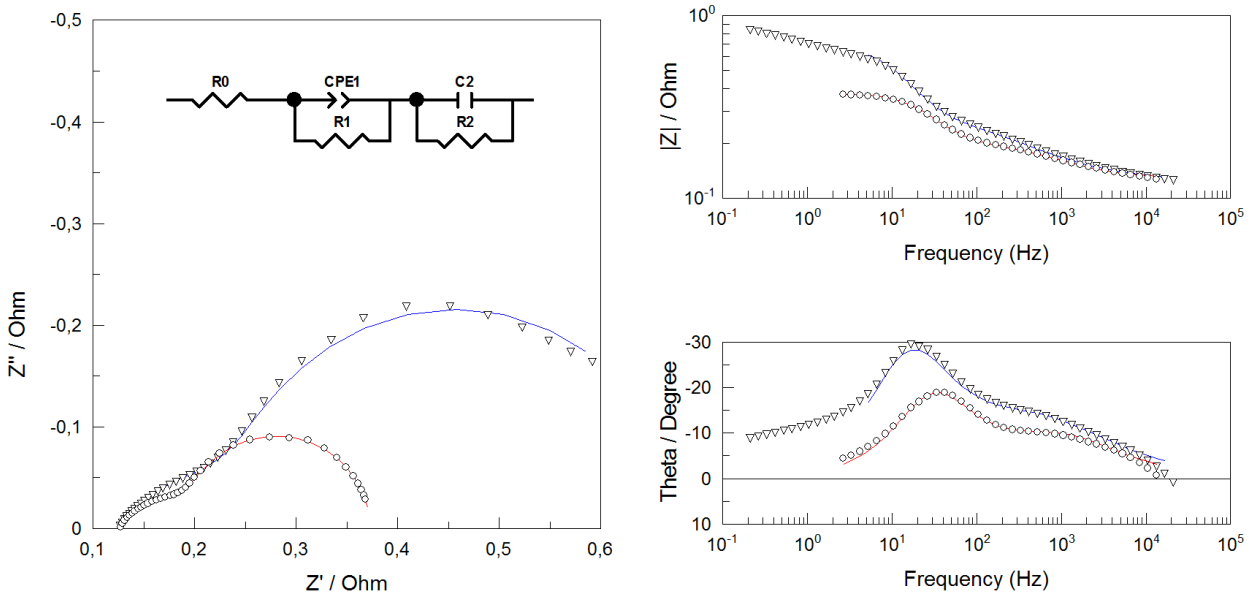

Figure 4.19: EC and fitting for 0.15 M solutions (triangles and blue line) and 0.3 M solutions (circles and red line) with flow rate of 16 mL/min

The constant phase element (CPE) is another component of the circuit which is an non-ideal capacitor. Its electrical impedance is defined as:

$$Z_{CPE} = \frac{1}{Y_0(j\,\omega)^n} \tag{4.4}$$

The parameter Y_0 and n (0<n<1) are independent on the frequency. For n=1 CPE consists of a pure capacitor while if n=0 it describes a pure resistor. A time constant is associated to the equivalent circuit shown in Figure 4.19. The time constant is characteristic for a loop where a resistor and a capacitor are placed in parallel, in this case the equivalent circuit will be characterized by two time constants. It is defined as:

$$\tau = RC \tag{4.5}$$

Where R is the resistance and C the capacitance. Two time constant can be evaluated for each circuit. They can directly be read from the Bode diagram in the plot of the phase angle. Each peak correspond to a time constant. In particular for the more concentrated solution the time constant for the high frequencies, equivalent to the circuit with the CPE and the resistor is 0.001 s and the time constant for the low frequencies which comprises the resistor and the capacitor is 0.28 s. Concerning the solution less concentrated the time constants are 0.0025 s and 0.625 s for low and high frequencies respectively.

Chapter 5

Discussion

This chapter has the objective to analyze and assess the results carrying out a comparison with what has been reported in literature.

The construction of the electrochemical cell was the most time consuming part of the work, from the choice of the best raw materials to the assembling process. Although there are several setups already commercialized the plan was to build up the cell minimizing the costs. Different setups and material have been tested in this work such as counter-flow inlet and outlet or interdigitated flow field in common graphite electrodes but without any success. Working with a device with acid solution flowing presented challenges in terms of leaking and corrosion issues. At the end the best configuration for a laboratory scale device was presented and tested in this work.

The polarization behaviour of VRFB was broadly treated in literature. It was observed the scan rate influenced the polarization curve with a proportional increase of the current density with an increase in the scan rate. This is confirmed by Hung et al. [84] that proves if the total variation of the polarization parameter in a period of time is the same, the frequency of increment had no effect on the polarization curves. Therefore, the main cause of the change in the electrochemical behaviour during polarization is due to the time to complete the polarization measurements. It causes significant reduction of redox active species in the electrolytes solutions.

The results presented in literature about the dependence of the performance on the electrolyte flow rate have a similar behaviour obtained in chapter 4. The current increases proportionally to the volume flow rate until an optimal flow rate, after which it is not convenient because of the electric power supplied to the peristaltic pump. This may be due to the absence of specific flow geometry which may ensure a good recirculation of the electrolytes inside the reactor. In fact, the enhancement in the performance of VRFB with flow field has also been investigated by Xu et al. [85]. In particular, the flow field plays an important role to limit the mass transport effect at low potentials, allow the cell to provide 250 mA/cm^2 for 1 M vanadium concentration in 3 M sulfuric acid.

Several carbon felt electrodes performance have been reported in literature. Although the non-treated electrode NATIONAL^{TM} Carbon Felt grade VGD tested in this work had worked with low concentration

of electrolytes, exhibited current density values between 150 and 250 mA/cm^2. Nibel et al. [86] have tested non treated electrodes with more concentrated electrolytes presenting results comparable to what obtained in this work. The charge-discharge cycles tests presented current efficiency with higher value compared to the reported values, but for the potential efficiency and the energy efficiency the value results to be lower [86]. From the results obtained in chapter 4 the current intensity has increased of 40% compared to the non-treated electrodes. A higher increment is presented by Eifert et al. [87] on different graphite felt electrodes which is between 50% and 180%. This might be due to the degradation of the fiber shown in SEM images. Although it may have increased the active area, on the other hand the graphite felt might not have been resisted to the exposition to the aggressive environment for such long time. Regarding the charge-discharge cycles and the related efficiency the remarkable enhancement is on the potential efficiency which affects the energy efficiency as well. Sun and Skyllas-Kazacos [76] obtained value comparable with the efficiency values recorded in this work. In particular for the more concentrated solution, the carbon felt used in this work exhibited a higher potential efficiency and energy efficiency.
The reason behind the better performance is still debated. Zeng et al. [88] studied the increment of functional group units amount as performance improvement compared to the increase on the active area.

The concentration of the electrolyte is crucial in the performance of the battery. The preparation of the electrolytes was carried out chemically. It was a simple and inexpensive method. The use of 0.3 M of vanadium which is just one third of the usual concentration used for energy storage showed good performance comparable with the literature. It may be because the electrode used has a large active area. Kim et al. [42] report tests on electrodes which have half of the thickness of the graphite felt used in this cell. The double amount of electroactive species had produced twice the current density and some times even three time more current density. Typical value of concentrations for operating VRFB are 1 M of vanadium in 2 or 3 M of sulfuric acid which lead to an increase in the potential of the cell according to Equation 2.14. Not only the vanadium ion concentration is important for the performance of the battery. The sulfuric acid concentration has a remarkable influence in the polarization curves, especially on the cell potential. In fact, according to Equation 2.14 the variation of the potential is about 120 mV/pH. Not only an increase in the voltage, Tsushima et al. [89] present an increase in the current density. In particular from 1 M to 4 M of H_2SO_4 concentration the current density increases from 85 mA/cm^2 to 200 mA/cm^2 for the same electrochemical cell configuration. With respect to the self-discharge behaviour, several studies have been presented aiming to understand the reagent crossover through the membrane, the main causes of self-discharge and contamination of the solutions. The outcome obtained in this work show a dependence of the self-discharge on the concentration of the reagents and the solvent. The more concentrated the solution is, more time will be necessary to register a drop in the potential due to vanadium ions crossover or water transport through the membrane. The result meets what has been reported in literature. Lawton et al. [90] show a dependence on concentration of the solvent and the solute. It affects the viscosity of the electrolytes making the crossover more difficult. In particular, doubling the concentration of sulfuric acid will increase by 50% the viscosity of the solutions [91].

To our knowledge the space-time characteristic of these cell has not been reported in literature. This is however an important parameter. It is deeply correlated with the fluid dynamics of the electrolyte inside the cell and it can be used to determine easily the conversion rate and to help define the optimal working conditions and an immediate way to understand how long the solution will remain inside the electrochemical reactor. It is also relevant to understand the mass effects inside the cell, especially when there is no flow geometry. From the Figure 4.1 some species are fast converted while some other take a longer path to come out probably because of stagnation points. The conversion efficiency has room to improvements.

The time evolution of the EIS tests shows an increment in the internal resistance of the cell which meets the results obtained by Jeong et al. [92]. The impedance spectra present a higher resistance when it comes to the solution with 0.15 M of V compared to the 0.3 M of V which meet the results obtained in the DC polarization curves. The membrane had shown a purely resistive behaviour during AC polarizations and the same outcome is obtained by Zago and Casalegno [93]. The EIS shows two capacitive loops, one at high frequencies and one at low frequencies respectively. The low frequency capacitive loop is assigned to the concentration influence, since it becomes smaller when the solution with the double of concentration is tested. It may be due to the electrode double layer of the transfer of the active species. The high frequency capacitive loop might be related to the contact resistance between the current collectors but further tests are needed in order to confirm this theory. Zago and Casalegno [93] shows two capacitive loops as well. With a mathematical model it relates the high frequency capacitive loop to the charge transfer phenomenon while the low frequency capacitive loop is due to diffusion and convection. In Nyquist plot the diffusion phenomenon appears to be a straight line which goes up to infinite and in the Bode plot as linear relationship between $\log(|Z|)$ versus $\log(\theta)$ with a slope value of 45 degrees, represented on the equivalent circuit as Warburg element and it is not present either in this work or in [93]. The EC resistance for the two different solutions presented in Table 4.4 correspond to the same value obtained from the polarization curves in DC at 16 mL/min flow rate listed in Table 4.1 and Table 4.2.
To our knowledge, most of the studies about EIS on VRFB have been conducted usually just in half-cell and consists of just one capacitive loop [83, 94, 95].

Conclusions

The vanadium redox flow battery was handmade from the raw material. Among the different conditions tested in this work, better performance were obtained through the use of the acid treated electrode and the solutions of 0.3 M.

Although the treatment with sulfuric acid presented some degradation on the carbon felt it exhibited improvement on the performance of the cell in terms of output power. The low concentration due to solubility constraint of the vanadium raw material was not a barrier because the output current densities obtained were comparable with the literature. The influence of the flow rate was found not relevant in solution with more concentration of active species. In particular the cell in its best configuration was characterized by a potential working range between 1.6 V and 1.2 V, a maximum output power of 40 mW/cm^2 and a energy efficiency of 81.4%.

It was possible to describe the electrochemical behaviour of the cell with an equivalent circuit. In particular it has been proven the pure resistive behaviour of the membrane.

At last, the objectives established at the beginning where all achieved, developing a small scale VRFB for energy storage with lower costs, although more test would have needed to be performed in order to better understand the mechanisms that occur into the electrochemical cell.

Perspective for future work

As there is not much reported in literature for a future work the attention should be focused on more EIS in order to comprehend the main causes behind the internal losses. Testing half-cell each time, different electrode thickness and concentration might help to evidence more the phenomena that occur inside the battery.

Further studies can be conducted on the different geometry of the cell in order to ensure a good recirculation and a uniform distribution of the reagents inside the cell, although a lot of studies have been conducted on this subject. The influence of the flow rate on different geometries can be analyzed in order to find a good compromise between the power supplied by the electrochemical cell and the power required for pumping the electrolytes, evaluating as well the hydraulic losses in the pipe circuit.

It would be interesting to test other treatments on the electrode, such as the microwave since it is very simple and inexpensive and try to investigate the influence of the active area on the current density and perform XPS to see the influence of the functional groups on the efficiency of the electrodes.

References

[1] W. Wang, L. Qingtao, B. Li, X. Wei, L. Li, and Z. Yang. Recent progress in redox flow battery research and development. *Adv. Funct. Mater.*, 2012. doi:10.1002/adfm.201200694.

[2] L. H. Thaller. US-Patent 3 996 064, 1976.

[3] Y. Zhao, M. Hong, N. B. Mercier, G. Yu, H. Choi, and H. Byon. A 3.5 V LithiumIodine Hybrid Redox Battery with vertically aligned carbon nanotube current collector. *Nano lett.*, 14(2):1085–1092, 2014. doi:10.1021/nl404784d.

[4] W. Li, Z. Liang, Z. Lu, X. Tao, K. Liu, H. Yao, and Y. Cui. Magnetic field-controlled lithium polysulfide semi-liquid battery with ferrofluidic properties. *Nano lett.*, 15(11):7394–7399, 2015. doi:10.1021/acs.nanolett.5b02818.

[5] W. Braff, M. Bazant, and C. Buie. Membrane-less hydrogen bromine flow battery. *Nat. Commun.*, 4(1), 2013. doi:10.1038/ncomms3346.

[6] M. Park, J. Ryu, W. Wang, and C. J. Material design and engineering of next-generation flow-battery technologies. *Nature Reviews Materials*, 2:16080, 2016. doi:10.1038/natrevmats.2016.80.

[7] M.Skyllas-Kazacos and F. Grossmith. Efficient vanadium redox flow cell. *J. Electrochem. Soc.*, 134: 2950–2953, 1987. doi:10.1149/1.2100321.

[8] D.-J. Park, K.-S. Jeon, C.-H. Ryu, and G.-J. Hwang. Performance of the all-vanadium redox flow battery stack. *J. Ind. Eng. Chem.*, 45:387–390, 2017. doi:10.1016/j.jiec.2016.10.007.

[9] D. Reed, E. Thomsen, B. Li, W. Wang, Z. Nie, B. Koeppel, and V. Sprenkle. Performance of a low cost interdigitated flow design on a 1 kw class all vanadium mixed acid redox flow battery. *J. Power Sources*, 306:24–31, 2016. doi:10.1016/j.jpowsour.2015.11.089.

[10] C. A. Vincent and B. Scrosati. *Modern batteries - An introduction to electrochemical power sources.* Butterworth-Heinemann, 2^{nd} edition, 1997. ISBN:0-340-66278-6.

[11] D. Pletcher. *Industrial electrochemistry.* Chapman and Hall, 1982. ISBN:0-412-16500-7.

[12] A. D. McNaught and A. Wilkinson. IUPAC. Compendium of Chemical Terminology, 2nd ed. (the "gold book"). Blackwell Scientific Publications, Oxford 1997. XML on-line corrected version: http://goldbook.iupac.org (2006-) created by M. Nic, J. Jirat, B. Kosata; updates compiled by A. Jenkins. ISBN 0-9678550-9-8. doi:10.1351/goldbook.

[13] C. H. Hamann, A. Hamnett, and W. Vielstich. *Electrochemistry*. WILEY-VCH Verlag GmbH and Co., second completely revised and updated edition, 2007. ISBN:978-3-527-31069-2.

[14] A. J. Bard and L. R. Faulkner. *Electrochemical Methods: Fundamentals and Applications*. Wiley, second edition, 2000. ISBN:978-0-471-04372-0.

[15] E. Gileadi, E. Kirowa-Eisner, and J. Penciner. *Interfacial Electrochemistry*. ADDISON-WESLEY publishing company, inc., 1975. ISBN:0-201-02399-9.

[16] C. Blanc. Modeling of a vanadium redox flow battery electricity storage system. PhD thesis n. 4277, École Polytechnique Fédérale de Lausanne, Switzerland. Apr 2009.

[17] C. Blanc and A. Rufer. Understanding the vanadium redox flow batteries. In book: Path to sustainable energy, Nov 2010. doi:10.5772/13338.

[18] P. A. Pissoort. FR-Patent 754 065, 1933.

[19] A. Pelligri and P. M. Spaziante. GB-Patent 2 030 349, 1978.

[20] M.Rychcik and M.Skyllas-Kazacos. Characteristics of a new all-vanadium redox flow battery. *J. Power Sources*, 22:59–67, 1988. doi:10.1016/0378-7753(88)80005-3.

[21] M. Skyllas-Kazacos, M. Rychcik, and R. Robins. AU-Patent 575 247, 1986.

[22] P. N. N. Laboratory. US-Patent 2015/0380757 A1, 2015.

[23] P. Alotto, M. Guarnieri, and F. Moro. Redox flow batteries for the storage of renewable energy: A review. *Renew. Sust. Energ. Rev.*, 29:325–335, 2014. doi:10.1016/j.rser.2013.08.001.

[24] J. Fu, M. Zheng, X. Wang, and J. Sun. Flow-rate optimization and economic analysis of vanadium redox flow batteries in a load-shifting application. *Journal of Energy Engineering*, 143, 2017. doi:10.1061/(ASCE)EY.1943-7897.0000493.

[25] A. Shah, M. Watt-Smith, and F. Walsh. A dynamic performance model for redox-flow batteries involving soluble species. *Electrochim. Acta*, 53:8087–8100, 2008. doi:10.1016/j.electacta.2008.05.067.

[26] R. Jervis, L. D. Brown, and T. Neville. Design of a miniature flow cell for in situ x-ray imaging of redox flow batteries. *J. Phys. D Appl. Phys.*, 49:43, 2016. doi:10.1088/0022-3727/49/43/434002.

[27] Z. Tang, D. S. Aaron, A. B. Papandrew, and T. A. Z. Jr. Monitoring the state of charge of operating vanadium redox flow batteries. *ECS Transactions*, 41:1–9, 2012. doi:10.1149/1.3697449.

[28] X. Qiu, T. Nguyen, J. Guggenberger, and M. Crow. A field validated model of a vanadium redox flow battery for microgrids. *IEEE Trans. Smart Grid*, 5(4):1592–1601, 2014. doi:10.1109/TSG.2014.2310212.

[29] B. Zakeri and S. Syri. Electrical energy storage systems: a comparative life cycle analysis. *Renew. Sust. Energ. Rev.*, 42:569–596, 2015. doi:j.rser.2014.10.011.

[30] A. Z. Weber, M. M. Mench, J. P. Meyers, P. N. Ross, J. T. Gostick, and Q. Liu. Redox flow batteries: A review. *J. Appl. Electrochem.*, 41:1137–1164, 2011. doi:10.1007/s10800-011-0348-2.

[31] M.Rychcik and M.Skyllas-Kazacos. Evaluation of electrode materials for vanadium redox cell. *J. Power Sources*, 19:45–54, 1987. doi:10.1016/0378-7753(87)80006-X.

[32] P. Leung, L. Xiaohong, C. P. de Leon, L. Berlouis, C. Law, and F. Walsh. Progress in redox flow batteries, remaining challenges and their applications in energy storage. *RSC Advances*, 2(27): 10125–10156, 2012. doi:10.1039/C2RA21342G.

[33] R. C. Engstrom and V. A. Strasser. Characterization of electrochemically pretreated glassy carbon electrodes. *Anal. Chem.*, 56:136–141, 1984. doi:10.1080/10618560701678647.

[34] L. J. Kepley and A. J. Bard. Ellipsometric, electrochemical, and elemental characterization of the surface phase produced on glassy carbon electrodes by electrochemical activation. *Anal. Chem.*, 60: 1459–1467, 1988. doi:10.1021/ac00165a022.

[35] R. L. M. Melanie. Poon and R. Engstrom. Laser activation of carbon electrodes. relationship between laser-induced surface effects and electron transfer activation. *Anal. Chem.*, 60:1725–1730, 1988. doi:10.1021/ac00168a018.

[36] N. Čėnas, J.Rozgaité, A.Pocius, and J.Kulys. Electrocatalytic oxidation of nadh and ascorbic acid on electrochemically pretreated glassy carbon electrodes. *J. Electroanal. Chem. Interfacial Electrochem.*, 154:121–128, 1983. doi:10.1016/S0022-0728(83)80535-X.

[37] R. M. Wightman, M. R. Deakin, P. M. Kovach, W. G. Kuhr, and K. J. Stutts. Methods to improve electrochemical reversibility at carbon electrodes. *J. Electrochem. Soc.*, 131:1578–1583, 1984. doi:10.1149/1.2115913.

[38] B. Sun and M. Skyllas-Kazacos. Modification of graphite electrode materials for VRFB applications - thermal treatment. *Electrochim. Acta*, 37(7):1253–1260, 1991. doi:10.1016/0013-4686(92)85064-R.

[39] S. Zhong and M. Skyllas-Kazacos. Electrochemical behaviour of vanadium(V)/vanadium(IV) redox couple at graphite electrodes. *J. Power Sources*, 39:1–9, 1992. doi:10.1016/0378-7753(92)85001-Q.

[40] C. Jian-Zhang, L. Wei-Yang, H. Wen-Yen, H. Cheng-Che, and C. Yong-Song. All-vanadium redox flow batteries with graphite felt electrodes treated by atmospheric pressure plasma jets. *J. Power Sources*, 274:307–327, 2015. doi:10.1016/j.jpowsour.2014.10.097.

[41] X. Wu, H. Xu, P. Xu, Y. Shen, L. Lu, J. Shi, J. Fu, and H. Zhao. Microwave-treated graphite felt as the positive electrode for all-vanadium redox ow battery. *J. Power Sources*, 263:104–109, 2014. doi:10.1016/j.jpowsour.2014.04.035.

[42] K. Kim, M. Park, Y. Kim, J. Kim, S. X. Dou, and M. Skyllas-Kazacos. A technology review of electrodes and reaction mechanisms in vanadium redox flow batteries. *J. Mater. Chem. A*, 33, 2015. doi:10.1039/c5ta02613j.

[43] H. Zhangxing, C. Zhongsheng, M. Wei, J. Yingqiao, C. Gang, D. Lei, and W. Ling. Modified carbon cloth as positive electrode with high electrochemical performance for vanadium redox flow batteries. *J. Energy Chem.*, 25:720–725, 2016. doi:10.1016/j.jechem.2016.04.002.

[44] S. Won, K. Oh, and H. Ju. Numerical studies of carbon paper-based vanadium redox ow batteries. *Electrochim. Acta*, 201:286–299, 2016. doi:10.1016/j.electacta.2015.11.091.

[45] A. M. Pezeshki, J. T. Clement, G. M. Veith, T. A. Zawodzinski, and M. M. Mench. High performance electrodes in vanadium redox flow batteries through oxygen-enriched thermal activation. *J. Power Sources*, 294:333–338, 2015. doi:10.1016/j.jpowsour.2015.05.118.

[46] G. Wei, W. Su, Z. Wei, X. Fan, J. Liu, and C. Yan. Electrocatalytic effect of the edge planes sites at graphite electrode on the vanadium redox couples. *Electrochim. Acta*, 204:263–269, 2016. doi:10.1016/j.electacta.2016.04.081.

[47] Vanadium-chemicals for the paint and ceramics industry. https://www.gfe.com/en/product-range/vanadium-chemicals/applications/paintceramics-industry/prettyPhoto, accessed 18 Aug 2018.

[48] F. Rahman. PhD Thesis, University of New South Wales, Sydney, Australia, 1998.

[49] M. Skyllas-Kazacos, M. Kazacos, and R. J. C. McDermott. Vanadium compound dissolution processes. Patent WO1989005363A1, 1988.

[50] M. Skyllas-Kazacos and M. Kazacos. Stabilised electrolyte solutions, methods of preparation thereof and redox cells and batteries containing stabilised electrolyte solutions. US Patent No. 6,143,443, 2000.

[51] F. Rahman and M. Skyllas-Kazacos. Vanadium redox battery: Positive half-cell electrolyte studies. *J. Power Sources*, 189:1212–1219, 2009. doi:10.1016/j.jpowsour.2008.12.113.

[52] T. Mohammadi and M. Skyllas-Kazacos. Evaluation of chemical stability of some membranes in vanadium solution. *J. Appl. Electrochem.*, 27:153–160, 1997. doi:10.1023/A:1018495722379.

[53] K. A. Mauritz and R. B. Moore. State of understanding of Nafion. *Chem. Rev.*, 104:4535–4586, 2004. doi:10.1021/cr0207123.

[54] T. Mohammadi, S. Chieng, and M. Skyllas-Kazacos. Water transport study across commercial ion exchange membranes in the vanadium redox flow battery. *J. Membr. Sci.*, 133:151–159, 1997. doi:10.1016/S0376-7388(97)00092-6.

[55] T. Mohammadi and M. Skyllas-Kazacos. Modification of anion-exchange membranes for vanadium redox battery applications. *J. Power Source*, 63:179–186, 1996. doi:10.1016/S0378-7753(96)02463-9.

[56] T. Sukkar and M. Skyllas-Kazacos. Water transfer behaviour across cation exchange membranes in the vanadium redox battery. *J. Membr. Sci.*, 222:235–247, 2003. doi:10.1016/S0376-7388(03)00309-0.

[57] J. Xi, Z. Wu, X. Qiu, and L. Chen. Nafion/SiO_2 hybrid membrane for vanadium redox ow battery. *J. Power Sources*, 166:531–536, 2007. doi:10.1016/j.jpowsour.2007.01.069.

[58] X. Teng, Y. Zhao, J. Xi, Z. Wu, and L. Chen. Nafon/organic silica modifed TiO2 composite membrane for vanadium redox ow battery via in situ sol-gel reactions. *J. Membr. Sci.*, 341:149–154, 2009. doi:10.1016/j.memsci.2009.05.051.

[59] S. Sang, Q. Wu, and K. Huang. Preparation of zirconium phosphate (ZrP)/ nafon1135 composite membrane and H^+/VO_2^+ transfer property investigation. *J. Membr. Sci.*, 305:118–124, 2007. doi:10.1016/j.memsci.2007.07.041.

[60] P. J. Hamilton and B. G. Pollet. Polymer electrolyte membrane fuel cell (pemfc) flow field plate: Design, materials and characterization. *Fuel Cells*, 10:489–509, 2010. doi:10.1002/fuce.201000033.

[61] X. Li and I. Sabir. Review of bipolar plates in pem fuel cells: Flow-field designs. *Int. J. Hydrogen Energy*, 30:359–371, 2005. doi:10.1016/j.ijhydene.2004.09.019.

[62] C. Yin, Y. Gao, S. Guo, and H. Tang. A coupled three dimensional model of vanadium redox flow battery for flow field designs. *Energy*, 74:886–895, 2014. doi:10.1016/j.energy.2014.07.066.

[63] R. L. Largent, M. Skyllas-Kazacos, and J. Chieng. Improved pv system performance using vanadium batteries. Proceedings IEEE 23rd Photovoltaic Specialists Conference, Louisville, Kentucky, US, 1993.

[64] M. Skyllas-Kazacos. Recent progress with the UNSW vanadium battery (online). http://www.arizonaenergy.org/Analysis/FuelCell/Vanadium%20Battery/recent_progress_with_the_unsw_va.htm, accessed 18 Jul 2018.

[65] C. Menictas and M. Skyllas-Kazacos. Small scale laboratory testing and golf-cart trials of 3 molar vanadium electrolyte. Report to Pinnacle VRB, pp. 60, 1998.

[66] S. Samuel. Vanadium flow battery energy storage. International Renewable Energy Storage Conference, Berlin, Germany, 2011.

[67] Office of Electricity Delivery and Energy Reliability. DOE global energy storage database (online). https://www.energystorageexchange.org/, accessed 04 Aug 2018.

[68] M. Schreiber, M. Harrer, A. Whitehead, H. Bucsich, M. Dragschitz, E. Seifert, and P. Tymciw. Practical and commercial issues in the design and manufacture of vanadium flow batteries. *J. Power Sources*, 206:483–489, 2012. doi:10.1016/j.jpowsour.2010.12.032.

[69] M. Schreiber and M. Harrer. Lifetime of vanadium redox flow batteries. Conference Cellstrom GmbH, IZNÖ-Süd Wr. Neudorf, Austria, 2011.

[70] T. Nguyen and R. Savinel. Flow batteries. *Electrochem. Soc. Interface*, 19:54–56, 2010. doi:10.1149/2.F06103if.

[71] L. Ren, Y. Tang, J. Shi, J. Dou, S. Zhou, and T. Jin. Techno-economic evaluation of hybrid energy storage technologies for a solar-wind generation system. *Physica C*, 484:272–275, 2013. doi:10.1016/j.physc.2012.02.048.

[72] A. Zahedi. Maximizing solar pv energy penetration using energy storage technology. *Renew. Sust. Energ. Rev.*, 15:866–867, 2011. doi:10.1016/j.rser.2010.09.011.

[73] Y. Zhang, S. Bao, T. Liu, T. Chen, and J. Huang. The technology of extracting vanadium from stone coal in china: History, current status and future prospects. *Hydrometallurgy*, 109:116–124, 2011. doi:10.1016/j.hydromet.2011.06.002.

[74] Q. Xu, T. Zhao, and P. Leung. Numerical investigation of flow field designs for vanadium redox flow batteries. *Appl. Energy*, 105:47–56, 2013. doi:10.1016/j.apenergy.2012.12.041.

[75] F. Xing, H. Zhang, and X. Ma. Shunt current loss of the vanadium redox flow battery. *J. Power Sources*, 196:10753–10757, 2011. doi:10.1016/j.jpowsour.2011.08.033.

[76] B. Sun and M. Skyllas-Kazacos. Chemical modification of graphite electrode materials for vanadium redox flow battery application - part ii. acid treatments. *Electrochim. Acta*, 13:2459–2465, 1992. doi:10.1016/0013-4686(92)87084-D.

[77] D. Aaron, Z. Tang, A. B. Papandrew, and T. A. Zawodzinski. Polarization curve analysis of all-vanadium redox flow batteries. *J. Appl. Electrochem.*, 41:1175–1182, 2011. doi:10.1007/s10800-011-0335-7.

[78] E. Agar, C. R. Dennison, K. W. Knehr, and E. C. Kumbur. Identification of performance limiting electrode using asymmetric cell configuration in vanadium redox flow batteries. *J. Power Sources*, 225:89–94, 2013. doi:10.1016/j.jpowsour.2012.10.016.

[79] C. Sun, F. Delnick, L. Baggetto, G. Veith, and T. Z. Jr. Hydrogen evolution at the negative electrode of the all-vanadium redox flow batteries. *J. Power Sources*, 248:560–564, 2014. doi:10.1016/j.jpowsour.2013.09.125.

[80] H. Liu, Q. Xu, C. Yan, and Y. Qiao. Corrosion behavior of a positive graphite electrode in vanadium redox flow battery. *Electrochim. Acta*, 56:8783–8790, 2011. doi:10.1016/j.electacta.2011.07.083.

[81] X. Yang, Q. Ye, P. Cheng, and T. Zhao. Effects of the electric field on ion crossover in vanadium redox flow batteries. *Appl. Energy*, 145:306–319, 2015. doi:10.1016/j.apenergy.2015.02.038.

[82] A. Lasia. *Electrochemical Impedance Spectroscopy and its Applications*. Springer, 2014. ISBN:978-1-4614-8932-0.

[83] C. Sun, F. Delnick, D. Aaron, A. Papandrew, M. Mench, and T. Zawodzinski. Resolving losses at the negative electode in all-vanadium redox flow batteries using electrochemical impedance spectroscopy. *J. Electrochem. Soc.*, 161:A981–A988, 2014. doi:10.1149/2.045406jes.

[84] Y. Hung, Y. Bu, J. Kubin, and D. Weinman. Effects of current scan rate on the polarization curve of vanadium redox flow batteries. *International Energy and Sustainability Conference (IESC)*, 2017. doi:10.1109/iesc.2017.8167489.

[85] Q. Xu, T. Zhao, and C. Zhang. Performance of a vanadium redox flow battery with and without flow field. *Electrochim. Acta*, 142:61–67, 2014. doi:10.1016/j.electacta.2014.07.059.

[86] O. Nibel, S. Taylor, S. Patru, A. Fabbri, E. Gubler, and T. Schmidt. Performance of different carbon electrode materials: Insights into stability and degradation under real vanadium redox flow battery operating conditions. *J. Electrochem. Soc.*, 164(7):A1608–A1615, 2017. doi:10.1149/2.1081707jes.

[87] L. Eifert, R. Banerjee, Z. Jusys, and R. Zeis. Characterization of carbon felt electrodes for vanadium redox flow batteries: Impact of treatment methods. *J. Electrochem. Soc.*, 165(11):A2577–A2586, 2018. doi:10.1149/2.0531811jes.

[88] L. Zeng, T. Zhao, and L. Wei. Revealing the performance enhancement of oxygenated carbonaceous materials for vanadium redox flow batteries: Functional groups or specific surface area? *Advanced sustainable systems*, 2(2), 2017. doi:10.1002/adsu.201700148.

[89] S. Tsushima, S. Sasaki, and S. Hirai. Influence of cell geometry and operating parameters on performance of a redox flow battery with serpentine and interdigitated flow fields. *ECS*, Meeting abstracts: 1164, 2013.

[90] J. Lawton, A. Jones, and T. Zawodzinski. Concentration dependence of vo2+ crossover of nafion for vanadium redox flow batteries. *J. Electrochem. Soc.*, 160(4):A697–A702, 2013. doi:10.1149/2.004306jes.

[91] F. H. Rhodes and C. B. Barbour. The viscosities of mixtures of sulfuric acid and water. *Ind. Eng. Chem.*, 15:850–852, 1923. doi:10.1021/ie50164a033.

[92] S. Jeong, L. Kim, Y. Kwon, and S. Kim. Effect of nafion membrane thickness on performance of vanadium redox flow battery. *Korean J. Chem. Eng.*, 31(11):2081–2087, 2014. doi:10.1007/s11814-014-0157-5.

[93] M. Zago and A. Casalegno. Physically-based impedance modeling of the negative electrode in all-vanadium redox flow batteries: insight into mass transport issues. *Electrochim. Acta*, 248:505–517, 2017. doi:10.1016/j.electacta.2017.07.166.

[94] J. Noack and J. Tubke. A comparison of materials and treatment of materials for vanadium redox flow battery. *ECS Transactions*, 25(35), 2010. doi:10.1149/1.3414022.

[95] I. Derr, M. Bruns, J. Lagner, A. Fetyan, J. Melke, and C. Roth. Degradation of all-vanadium redox flow batteries (vrfb) investigated by electrochemical impedance and x-ray photoelectron spectroscopy: Part 2 electrochemical degradation. *J. Power Sources*, 325:351–359, 2016. doi:10.1016/j.jpowsour.2016.06.040.